Marine Systems & Ocean Technology (2023) 18:89–110
https://doi.org/10.1007/s40868-023-00126-5

ORIGINAL PAPER

A nonlinear optimal control approach for unmanned surface vessels

G. Rigatos[1]

Received: 21 November 2022 / Accepted: 29 June 2023 / Published online: 21 December 2023

Abstract
The ability of unmanned surface vessels for performing dexterous maneuvering is important for improving vessels' safety, reliability and operational capacity. The article proposes a nonlinear optimal control approach for unmanned surface vessels. These vessels exhibit three degrees of freedom while their dynamic model can be formulated in analogy to the one of robotic manipulators. This model undergoes approximate linearization around a temporary operating point that is recomputed at each time-step of the control method. The linearization relies on Taylor series expansion and on the associated Jacobian matrices. For the linearized state-space model of the system a stabilizing optimal (H-infinity) feedback controller is designed. This controller stands for the solution to the nonlinear optimal control problem under model uncertainty and external perturbations. To compute the controller's feedback gains an algebraic Riccati equation is repetitively solved at each iteration of the control algorithm. The stability properties of the control method are proven through Lyapunov analysis. Finally, to implement state estimation-based control without the need to measure the entire state vector of the vessel, the H-infinity Kalman Filter is used as a robust state estimator. The article's results can be extended to the case of underactuation, that is when the 3-DOF vessel has no thrusters to enable propulsion along its transversal axis. The solution of the nonlinear optimal control problem for unmanned surface vessels allows for reducing energy consumption by their propulsion and navigation system and thus it permits to improve the vessels' autonomy and operational capacity.

Keywords Unmanned surface vessels · Autonomous ships · 3-DOF ship motion · Nonlinear H-infinity control · Taylor series expansion · Jacobian matrices · Riccati equation · Global stability

1 Introduction

The solution of the nonlinear optimal control problem for 3-DOF unmanned surface vessels (USVs) remains always a technical challenge [1–4]. The dynamic model of 3-DOF USVs is a highly nonlinear and multivariable one [5–7]. The vessel's model can be fully actuated (when receiving as control inputs the engine's forward propulsion, the rudder's torque and the thrusters' lateral propulsion. On the other side this dynamic model can be underactuated when thrusters' lateral propulsion is missing [8–10]. Solution of the control problem for USVs enables autonomous navigation of the individual vessels or coordination of multiple vessels' motion [11–13]. Several nonlinear control approaches, including robust and adaptive control schemes, have been developed. Precise tracking of reference setpoints and global stability properties of the USVs control loop are the design objectives in all related nonlinear control methods. Results on autonomous navigation of USVs with the use of adaptive control methods can be found in [14–17]. Results on the use of sliding-mode and robust control methods for solving the autonomous navigation problem of USVs are given in [18–21]. The use of observers and disturbance estimators in control loops of USVs can be found in [12–24]. Additional results on nonlinear control of 3-DOF USVs under disturbances can be found in [25–28]. Besides, recent developments on USV control under model uncertainty and perturbations are given in [29–31].

In the present article, a new nonlinear optimal control approach is developed for the dynamic model of 3-DOF unmanned surface vessels (USVs) [1]. This model is in the typical form of a robotic system, comprising an inertia matrix, a Coriolis and a centrifugal forces matrix, while receiving inputs from propulsion forces and rudder torques. It is shown that this model can be written in the

✉ G. Rigatos
grigat@ieee.org

[1] Unit of Industrial Automation, Industrial Systems Institute, 26504 Rion Patras, Greece

affine-in-the-input nonlinear state-space form. Besides, it is proven that in the case of full actuation it satisfies differential flatness properties. Next, the dynamic model of the 3-DOF USV undergoes approximate linearization with the use of first-order Taylor series expansion and through the computation of the associated Jacobian matrices [32–35]. Linearization takes place around a temporary operating point which is recomputed at each time-step of the control algorithm. This operating point is redefined at each sampling instance by the present value of the USV's state vector and by the last sampled value of the control inputs vector. The modelling error which is due to truncation of higher-order terms in the Taylor series expansion is viewed as a perturbation that is asymptotically compensated by the robustness of the control algorithm.

For the approximately linearized dynamic model of the 3-DOF USV a stabilizing H-infinity feedback controller is designed [1]. This controller achieves the solution of the optimal control problem for the dynamics of the 3-DOF USV under model uncertainties and external disturbances. It can be stated that the H-infnity-controller represents a min-max differential game taking place between (i) the control inputs of the USV which try to minimize a quadratic cost function of the state vector's tracking error and (ii) the model uncertainty and external disturbance terms which try to maximize this cost function. To select the stabilizing feedback gains of the H-infinity controller an algebraic Riccati equation is repetitively solved at each time-step of the control method [36–38]. The global stability properties of the control scheme are proven through Lyapunov analysis. First, it is demonstrated that the control loop of the USV satisfies the H-infinity tracking performance criterion [1, 39]. This signifies elevated robustness under model imprecision and external perturbations. Additionally, to implement state estimation-based control without the need to measure the entire state vector of the USV, the H-infinity Kalman Filter is used as a robust state estimator [1, 40].

The proposed nonlinear optimal control method retains the known advantages of linear optimal control, that is fast and accurate tracking of reference setpoints under moderate variations of the control inputs. Comparing to past attempts to solve the nonlinear optimal (H-infinity) control problem, the following advancements can be noted: (i) in past results, the linearization of the system's dynamics is performed at points of the desirable trajectories (setpoints), whereas in the article's control method linearization is performed around a time-varying operating point which is redefined at each sampling instance by the present value of the system's state vector and by the last sampled value of the control inputs vector, (ii) in past results the system is considered to be exclusively in the affine-in-the-input state-space form with a control inputs gain matrix which is time-invariant. On the contrary, in the present article's approach there is no constraint to find the system in the affine-in-the-input state space form, while even in such a state-space description the control inputs gain matrix can be time-varying, (iii) in past approaches a different Lyapunov analysis procedure has been used to prove stability properties. In the present article, a novel Lyapunov function has been introduced to prove the global stability properties of the nonlinear optimal control scheme.

The structure of the article is defined as follows: in Sect. 2 the nonlinear dynamic model of the 3-DOF USV is formulated. The differential flatness properties of the model are proven. In Sect. 3 the dynamic model of the USV undergoes approximate linearization with the use of first-order Taylor series expansion and through the computation of the associated Jacobian matrices. In Sect. 4 the global stability properties of the control scheme are proven through Lyapunov analysis. In Sect. 5 the fine performance of the control method is further confirmed through simulation experiments. Finally, in Sect. 6 concluding remarks are stated.

2 Dynamic model of the unmanned surface vessel

2.1 Dynamics of the USV

The motion of the Unmanned Surface Vessle (USV) is described in both a body-fixed reference frame and in an inertial (earth-fixed) reference frame (Fig 1). In the body-fixed reference frame the joint kinematic and dynamic model of the USV comprises the following two-equations in matrix form [1, 3, 36]:

$$\begin{aligned} &\dot{\eta} = R(\psi)v \Rightarrow \dot{v} = R^{-1}(\psi)\dot{\eta} \\ &M\dot{v} + Dv = \tau \end{aligned} \tag{1}$$

where $\eta(t) = [x(t)\ y(t)\ \psi(t)]^T \in R^{3\times 1}$ are the cartesian coordinates and the orientation angle of the vessel in the inertial reference frame *OXYZ*. The associate velocities vector in the inertial reference frame is $\dot{\eta}(t) = [\dot{x}(t)\ \dot{y}(t)\ \dot{\psi}(t)]^T \in R^{3\times 1}$. The velocities vector in the body-fixed reference frame $\Sigma V_1 V_2 V_3$ is denoted as $v(t) = [v_1\ v_2\ v_3]^T$ where v_1 is the surge velocity, v_2 is the sway velocity and v_3 is the yaw turn velocity of the vessel.

In the above model, matrices M, D and R are given by [1, 3, 36]

$$\begin{aligned} M &= \begin{pmatrix} m_{11} & 0 & 0 \\ 0 & m_{22} & m_{33} \\ 0 & m_{23} & m_{33} \end{pmatrix} D = \begin{pmatrix} d_{11} & 0 & 0 \\ 0 & d_{22} & d_{23} \\ 0 & d_{22} & d_{33} \end{pmatrix} \\ R &= \begin{pmatrix} cos(\psi) & -sin(\psi) & 0 \\ sin(\psi) & cos(\psi) & 0 \\ 0 & 0 & 1 \end{pmatrix} \end{aligned} \tag{2}$$

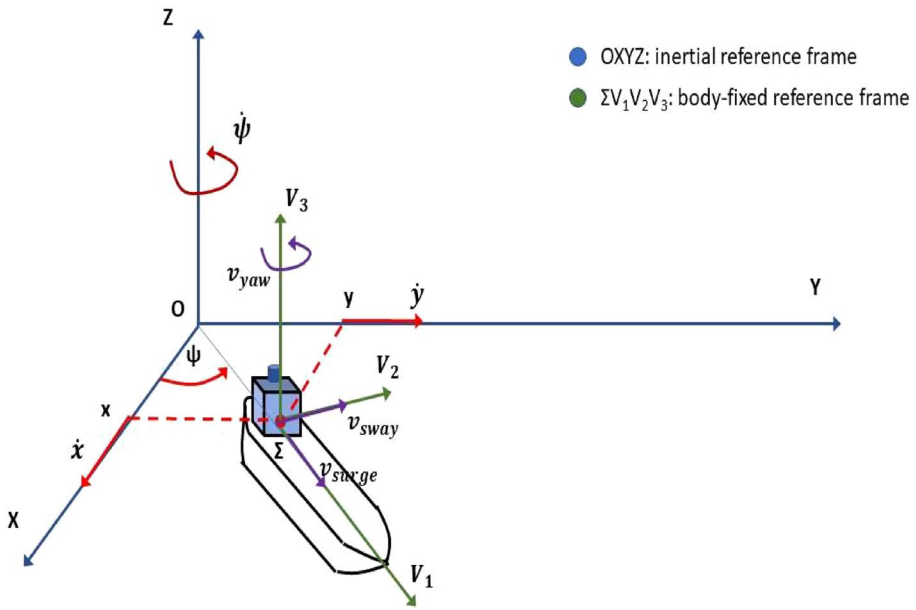

Fig. 1 Monitoring of the motion of the USV in an inertial reference frame *OXYZ* as well as in a body-fixed reference $\Sigma V_1 V_2 V_3$

The dynamic model of the USV is expressed next exclusively in the inertial reference frame. Using the previous relations it holds that [1, 3, 36]

$$\tilde{J}\ddot{\eta} + \tilde{C}(\eta,\dot{\eta})\dot{\eta} + \tilde{F}\dot{\eta} = \tau^* \tag{3}$$

where $\tilde{J} = RMR^T \in R^{3\times3}$, $\tilde{C}(\eta,\dot{\eta}) = RM\dot{R}^T \in R^{3\times3}$, $\tilde{F} = RDR^T \in R^{3\times3}$ and $\tau^* = R\tau \in R^{3\times1}$. It holds that

$$\tilde{J}(\eta) = \begin{pmatrix} m_{11}cos^2(\psi) + m_{22}sin^2(\psi) & (m_{11} - m_{22})sin(\psi)cos(\psi) & -m_{23}sin(\psi) \\ (m_{11} - m_{22})sin(\psi)cos(\psi) & m_{11}sin^2(\psi) + m_{22}cos^2(\psi) & m_{23}cos(\psi) \\ -m_{23}sin(\psi) & m_{23}cos(\psi) & m_{33} \end{pmatrix} \tag{4}$$

$$\tilde{C}(\eta,\dot{\eta}) = \begin{pmatrix} \dot{\psi}(m_{22} - m_{11})sin(\psi)cos(\psi) & \dot{\psi}(m_{11}cos^2(\psi) + m_{22}sin^2(\psi)) & 0 \\ -\dot{\psi}(m_{11}sin^2(\psi) + m_{22}cos^2(\psi)) & \dot{\psi}(m_{11} - m_{22})sin(\psi)cos(\psi) & 0 \\ -\dot{\psi}m_{23}cos(\psi) & -\dot{\psi}m_{23}sin(\psi) & 0 \end{pmatrix} \tag{5}$$

$$\tilde{F}(\eta) = \begin{pmatrix} d_{11}cos^2(\psi) + d_{22}sin^2(\psi) & (d_{11} - d_{22})sin(\psi)cos(\psi) & -d_{23}sin(\psi) \\ (d_{11} - d_{22})sin(\psi)cos(\psi) & d_{11}sim^2(\psi) + d_{22}cos^2(\psi) & d_{23}cos(\psi) \\ -d_{32}sin(\psi) & d_{22}cos(\psi) & d_{23} \end{pmatrix} \tag{6}$$

Using Eq. (3) the dynamic model of the USV can be written as [1, 3, 36]

$$\begin{aligned} &\tilde{J}(\eta)\ddot{\eta} + \tilde{C}(\eta,\dot{\eta})\dot{\eta} + \tilde{F}(\eta)\dot{\eta} = \tau^* \Rightarrow \\ &\ddot{\eta} = -\tilde{J}^{-1}(\eta)\tilde{C}(\eta,\dot{\eta})\dot{\eta} \\ &-\tilde{J}^{-1}(\eta)\tilde{F}(\eta)\dot{\eta} + \tilde{J}^{-1}(\eta)\tau^* \Rightarrow \\ &\ddot{\eta} = -\tilde{J}^{-1}(\eta)[\tilde{C}(\eta,\dot{\eta}) + \tilde{F}(\eta)]\dot{\eta} + \tilde{J}^{-1}\tau^* \end{aligned} \tag{7}$$

The inverse matrix $\tilde{J}^{-1}(\eta)$ is computed first. It holds that

$$\tilde{J}(\eta) = \begin{pmatrix} \tilde{J}_{11} & \tilde{J}_{12} & \tilde{J}_{13} \\ \tilde{J}_{21} & \tilde{J}_{22} & \tilde{J}_{23} \\ \tilde{J}_{31} & \tilde{J}_{32} & \tilde{J}_{33} \end{pmatrix} \tag{8}$$

with $\tilde{J}_{11} = m_{11}cos^2(\psi) + m_{22}sin^2(\psi)$, $\tilde{J}_{12} = (m_{11} - m_{22})sin(\psi)cos(\psi)$, $\tilde{J}_{13} = -m_{23}sin(\psi)$, $\tilde{J}_{21} = (m_{11} - m_{22})sin(\psi)cos(\psi)$, $\tilde{J}_{22} = m_{11}sin^2(\psi) + m_{22}cos^2(\psi)$, $\tilde{J}_{23} = m_{23}cos(\psi)$, $\tilde{J}_{31} = -m_{23}sin(\psi)$, $\tilde{J}_{32} = m_{23}cos(\psi)$ and $J_{33} = m_{33}$.

The determinant of matrix $\tilde{J}(\eta,\dot{\eta})$ is

$$\begin{aligned} detJ = &\tilde{J}_{11}(\tilde{J}_{22}\tilde{J}_{33} - \tilde{J}_{32}\tilde{J}_{23}) - \\ &-\tilde{J}_{12}(\tilde{J}_{21}\tilde{J}_{33} - \tilde{J}_{31}\tilde{J}_{23}) + \\ &+\tilde{J}_{13}(\tilde{J}_{21}\tilde{J}_{32} - \tilde{J}_{31}\tilde{J}_{22}) \end{aligned} \tag{9}$$

The sub-determinants of matrix $\tilde{J}(\eta,\dot{\eta})$ are defined as: $J_{11}=\tilde{J}_{22}\tilde{J}_{33}-\tilde{J}_{32}\tilde{J}_{23}$, $J_{12}=\tilde{J}_{21}\tilde{J}_{33}-\tilde{J}_{31}\tilde{J}_{23}$, $J_{13}=\tilde{J}_{21}\tilde{J}_{32}-\tilde{J}_{31}\tilde{J}_{22}$, $J_{21}=\tilde{J}_{12}\tilde{J}_{33}-\tilde{J}_{32}\tilde{J}_{13}$, $J_{22}=\tilde{J}_{11}\tilde{J}_{33}-\tilde{J}_{31}\tilde{J}_{13}$, $J_{23}=\tilde{J}_{11}\tilde{J}_{22}-\tilde{J}_{31}\tilde{J}_{12}$, $J_{31}=\tilde{J}_{12}\tilde{J}_{23}-\tilde{J}_{22}\tilde{J}_{13}$, $J_{32}=\tilde{J}_{11}\tilde{J}_{23}-\tilde{J}_{21}\tilde{J}_{13}$, $J_{33}=\tilde{J}_{11}\tilde{J}_{22}-\tilde{J}_{21}\tilde{J}_{12}$.

Thus, the inverse of matrix $\tilde{J}(\eta)$ is

$$\tilde{J}^{-1}(\eta)=\frac{1}{det\tilde{J}}\begin{pmatrix}J_{11}&-J_{21}&J_{31}\\-J_{12}&J_{22}&-J_{32}\\J_{13}&-J_{23}&J_{33}\end{pmatrix} \tag{10}$$

Moreover the vector of the Coriolis and centrifugal forces $\tilde{C}(\eta,\dot{\eta})\dot{\eta}$ is written in the following form

$$C(\eta,\dot{\eta})=\begin{pmatrix}c_1\\c_2\\c_3\end{pmatrix}=\begin{pmatrix}\tilde{C}_{11}\dot{\eta}_1+\tilde{C}_{12}\dot{\eta}_2+\tilde{C}_{13}\dot{\eta}_3\\\tilde{C}_{21}\dot{\eta}_1+\tilde{C}_{22}\dot{\eta}_2+\tilde{C}_{23}\dot{\eta}_3\\\tilde{C}_{31}\dot{\eta}_1+\tilde{C}_{32}\dot{\eta}_2+\tilde{C}_{33}\dot{\eta}_3\end{pmatrix} \tag{11}$$

where $\tilde{C}_{11}=\dot{\psi}(m_{22}-m_{11})sin(\psi)cos(\psi)$, $\tilde{C}_{12}=\dot{\psi}(m_{11}cos^2(\psi)+m_{22}sin^2(\psi))$, $\tilde{C}_{13}=0$, $\tilde{C}_{21}=-\dot{\psi}(m_{11}sin^2(\psi)+m_{22}cos^2(\psi))$, $\tilde{C}_{22}=\dot{\psi}(m_{11}-m_{22})sin(\psi)cos(\psi)$, $\tilde{C}_{23}=0$, $\tilde{C}_{31}=-\dot{\psi}m_{23}cos(\psi)$, $\tilde{C}_{32}=-\dot{\psi}m_{23}sin(\psi)$, $\tilde{C}_{33}=0$.

Additionally, the damping forces vector $\tilde{F}(\eta)\dot{\eta}$ can be written in the form:

$$Q(\eta,\dot{\eta})=\begin{pmatrix}q_1\\q_2\\q_3\end{pmatrix}=\begin{pmatrix}\tilde{F}_{11}\dot{\eta}_1+\tilde{F}_{12}\dot{\eta}_2+\tilde{F}_{13}\dot{\eta}_3\\\tilde{F}_{21}\dot{\eta}_1+\tilde{F}_{22}\dot{\eta}_2+\tilde{F}_{23}\dot{\eta}_3\\\tilde{F}_{31}\dot{\eta}_1+\tilde{F}_{32}\dot{\eta}_2+\tilde{F}_{33}\dot{\eta}_3\end{pmatrix} \tag{12}$$

where $\tilde{F}_{11}=d_{11}cos^2(\psi)+d_{22}sin^2(\psi)$, $\tilde{F}_{12}=(d_{11}-d_{22})sin(\psi)cos(\psi)$, $\tilde{F}_{13}=-d_{23}sin(\psi)$, $\tilde{F}_{21}=(d_{11}-d_{22})sin(\psi)cos(\psi)$, $\tilde{F}_{22}=d_{11}sim^2(\psi)+d_{22}cos^2(\psi)$, $\tilde{F}_{23}=d_{23}cos(\psi)$, $\tilde{F}_{31}=-d_{32}sin(\psi)$, $\tilde{F}_{32}=d_{22}cos(\psi)$, $\tilde{F}_{33}=d_{23}$.

Consequently, the dynamic model of the autonomous surface vessel is written as

$$\ddot{\eta}=-\tilde{J}^{-1}(\eta)C(\eta,\dot{\eta})-\tilde{J}^{-1}(\eta)Q(\eta,\dot{\eta})+\tilde{J}^{-1}(\eta)\tau^{*} \tag{13}$$

or equivalently

$$\begin{aligned}\begin{pmatrix}\ddot{\eta}_1\\\ddot{\eta}_2\\\ddot{\eta}_3\end{pmatrix}&=-\frac{1}{det\tilde{J}}\begin{pmatrix}J_{11}&-J_{21}&J_{31}\\-J_{12}&J_{22}&-J_{32}\\J_{13}&-J_{23}&J_{33}\end{pmatrix}\begin{pmatrix}c_1\\c_2\\c_3\end{pmatrix}\\&-\frac{1}{det\tilde{J}}\begin{pmatrix}J_{11}&-J_{21}&J_{31}\\-J_{12}&J_{22}&-J_{32}\\J_{13}&-J_{23}&J_{33}\end{pmatrix}\begin{pmatrix}q_1\\q_2\\q_3\end{pmatrix}+\\&+\frac{1}{det\tilde{J}}\begin{pmatrix}J_{11}&-J_{21}&J_{31}\\-J_{12}&J_{22}&-J_{32}\\J_{13}&-J_{23}&J_{33}\end{pmatrix}\begin{pmatrix}\tau_1\\\tau_2\\\tau_3\end{pmatrix}\end{aligned} \tag{14}$$

or similarly

$$\begin{aligned}\begin{pmatrix}\ddot{\eta}_1\\\ddot{\eta}_2\\\ddot{\eta}_3\end{pmatrix}&=-\frac{1}{det\tilde{J}}\begin{pmatrix}J_{11}&-J_{21}&J_{31}\\-J_{12}&J_{22}&-J_{32}\\J_{13}&-J_{23}&J_{33}\end{pmatrix}\begin{pmatrix}c_1+q_1\\c_2+q_2\\c_3+q_3\end{pmatrix}\\&+\frac{1}{det\tilde{J}}\begin{pmatrix}J_{11}&-J_{21}&J_{31}\\-J_{12}&J_{22}&-J_{32}\\J_{13}&-J_{23}&J_{33}\end{pmatrix}\begin{pmatrix}\tau_1\\\tau_2\\\tau_3\end{pmatrix}\end{aligned} \tag{15}$$

Consequently, the dynamic model of the unmanned surface vessel can be written as

$$\begin{aligned}\begin{pmatrix}\ddot{\eta}_1\\\ddot{\eta}_2\\\ddot{\eta}_3\end{pmatrix}&=\begin{pmatrix}\frac{-J_{11}(c_1+q_1)+J_{21}(c_2+q_2)-J_{31}(c_3+q_3)}{detJ}\\\frac{J_{12}(c_1+q_1)-J_{22}(c_2+q_2)+J_{32}(c_3+q_3)}{detJ}\\\frac{-J_{13}(c_1+q_1)+J_{23}(c_2+q_2)-J_{33}(c_3+q_3)}{detJ}\end{pmatrix}+\begin{pmatrix}\frac{J_{11}}{detJ}\\-\frac{J_{12}}{detJ}\\\frac{J_{13}}{detJ}\end{pmatrix}\\&\tau_1+\begin{pmatrix}-\frac{J_{21}}{detJ}\\\frac{J_{22}}{detJ}\\-\frac{J_{23}}{detJ}\end{pmatrix}\tau_2+\begin{pmatrix}\frac{J_{31}}{detJ}\\-\frac{J_{32}}{detJ}\\\frac{J_{33}}{detJ}\end{pmatrix}\tau_3\end{aligned} \tag{16}$$

Next, the following state vector is defined for the USV $x=[x_1,x_2,x_3,x_4,x_5,x_6,x_7,x_8]^T$,or$x=[\eta_1,\dot{\eta}_1,\eta_2,\dot{\eta}_2,\eta_3,\dot{\eta}_3]^T$, that is $x=[x,\dot{x},y,\dot{y},\psi,\dot{\psi}]^T$. Besides, the control inputs vector is defined as $u=[u_1,u_2,u_3]^T$ or $u=[\tau_1,\tau_2,\tau_3]^T$. Then, the dynamic model of the USV is written as

$$\begin{aligned}\begin{pmatrix}\dot{x}_1\\\dot{x}_2\\\dot{x}_3\\\dot{x}_4\\\dot{x}_5\\\dot{x}_6\end{pmatrix}&=\begin{pmatrix}x_2\\\frac{-J_{11}(c_1+q_1)+J_{21}(c_2+q_2)-J_{31}(c_3+q_3)}{detJ}\\x_4\\\frac{J_{12}(c_1+q_1)-J_{22}(c_2+q_2)+J_{32}(c_3+q_3)}{detJ}\\x_6\\\frac{-J_{13}(c_1+q_1)+J_{23}(c_2+q_2)-J_{33}(c_3+q_3)}{detJ}\end{pmatrix}+\begin{pmatrix}0\\\frac{J_{11}}{detJ}\\0\\-\frac{J_{12}}{detJ}\\0\\\frac{J_{13}}{detJ}\end{pmatrix}\\&u_1+\begin{pmatrix}0\\-\frac{J_{21}}{detJ}\\0\\\frac{J_{22}}{detJ}\\0\\-\frac{J_{23}}{detJ}\end{pmatrix}u_2+\begin{pmatrix}0\\\frac{J_{31}}{detJ}\\0\\-\frac{J_{32}}{detJ}\\0\\\frac{J_{33}}{detJ}\end{pmatrix}u_3\end{aligned} \tag{17}$$

Thus, the dynamic model of the USV is written in the following nonlinear affine-in-the-input state-space form:

$$\dot{x}=f(x)+g_1(x)u_1+g_2(x)u_2+g_3(x)u_3 \tag{18}$$

with $x\in R^{6\times1}$, $f(x)\in R^{6\times1}$, $g_1(x)\in R^{6\times1}$, $g_2(x)\in R^{6\times1}$, $g_3(x)\in R^{6\times1}$ and $u\in R^{3\times1}$. Next, the elements of the state-space description

of the USV are written as functions of the state vector elements x_1 to x_6.

Thus $J_{11} = m_{11}cos^2(x_5) + m_{22}sin^2(x_5)$,
$J_{12} = (m_{11} - m_{22})sin(x_5)cos(x_5)$,
$J_{13} = -m_{23}sin(x_5)$, $J_{21} = (m_{11} - m_{22})sin(x_5)cos(x_5)$,
$J_{22} = m_{11}sin^2(x_5) + m_{22}cos^2(x_5)$, $J_{23} = m_{23}cos(x_5)$,
$J_{31} = -m_{23}sin(x_5)$, $J_{32} = m_{23}cos(x_5)$ and $J_{33} = m_{33}$.

and $\tilde{C}_{11} = x_6(m_{22} - m_{11})sin(x_5)cos(x_5)$,
$\tilde{C}_{12} = x_6(m_{11}cos^2(x_5) + m_{22}sin^2(x_5))$, $\tilde{C}_{13} = 0$,
$\tilde{C}_{21} = -x_6(m_{11}sin^2(x_5) + m_{22}cos^2(x_5))$,
$\tilde{C}_{22} = x_6(m_{11} - m_{22})sin(x_5)cos(x_5)$, $\tilde{C}_{23} = 0$,
$\tilde{C}_{31} = -x_6m_{23}cos(x_5)$, $\tilde{C}_{32} = -x_6m_{23}sin(x_5)$, $\tilde{C}_{33} = 0$.

and $\tilde{F}_{11} = d_{11}cos^2(x_5) + d_{22}sin^2(x_5)$,
$\tilde{F}_{12} = (d_{11} - d_{22})sin(x_5)cos(x_5)$,
$\tilde{F}_{13} = -d_{23}sin(x_5)$, $\tilde{F}_{21} = (d_{11} - d_{22})sin(x_5)cos(x_5)$,
$\tilde{F}_{22} = d_{11}sim^2(x_5) + d_{22}cos^2(x_5)$, $\tilde{F}_{23} = d_{23}cos(x_5)$,
$\tilde{F}_{31} = -d_{32}sin(x_5)$, $\tilde{F}_{32} = d_{22}cos(x_5)$, $\tilde{F}_{33} = d_{23}$.

2.2 Differential flatness properties of the USV dynamic model

It will be proven that the dynamic model of the 3-DOF USV is differentially flat with flat outputs vector $y = [x, y, \psi]^T$ of $y = [x_1, x_3, x_5]^T$. From the first, third and fifth rows of the state-space model of the USV one obtains

$$x_2 = \dot{x}_1 \;\; x_4 = \dot{x}_3 \;\; x_6 = \dot{x}_5 \tag{19}$$

This signifies that all state variables of the USV can be written as differential functions of the system's flat outputs. Besides, the state-space model of the USV can be written as

$$\begin{pmatrix} \ddot{x}_1 \\ \ddot{x}_3 \\ \ddot{x}_5 \end{pmatrix} = \begin{pmatrix} \frac{-J_{11}(c_1+q_1)+J_{21}(c_2+q_2)-J_{31}(c_3+q_3)}{detJ} \\ \frac{J_{12}(c_1+q_1)-J_{22}(c_2+q_2)+J_{32}(c_3+q_3)}{detJ} \\ \frac{J_{13}(c_1+q_1)-J_{23}(c_2+q_2)+J_{33}(c_3+q_3)}{detJ} \end{pmatrix} + \begin{pmatrix} \frac{J_{11}}{detJ} & -\frac{J_{21}}{detJ} & \frac{J_{31}}{detJ} \\ -\frac{J_{12}}{detJ} & \frac{J_{22}}{detJ} & -\frac{J_{32}}{detJ} \\ \frac{J_{13}}{detJ} & -\frac{J_{23}}{detJ} & \frac{J_{33}}{detJ} \end{pmatrix} \begin{pmatrix} u_1 \\ u_2 \\ u_3 \end{pmatrix} \tag{20}$$

or equivalently

$$\begin{pmatrix} u_1 \\ u_2 \\ u_3 \end{pmatrix} = \begin{pmatrix} \frac{J_{11}}{detJ} & -\frac{J_{21}}{detJ} & \frac{J_{31}}{detJ} \\ -\frac{J_{12}}{detJ} & \frac{J_{22}}{detJ} & -\frac{J_{32}}{detJ} \\ \frac{J_{13}}{detJ} & -\frac{J_{23}}{detJ} & \frac{J_{33}}{detJ} \end{pmatrix}^{-1} \left[\begin{pmatrix} \ddot{x}_1 \\ \ddot{x}_3 \\ \ddot{x}_5 \end{pmatrix} - \begin{pmatrix} \frac{-J_{11}(c_1+q_1)+J_{21}(c_2+q_2)-J_{31}(c_3+q_3)}{detJ} \\ \frac{J_{12}(c_1+q_1)-J_{22}(c_2+q_2)+J_{32}(c_3+q_3)}{detJ} \\ \frac{-J_{13}(c_1+q_1)+J_{23}(c_2+q_2)-J_{33}(c_3+q_3)}{detJ} \end{pmatrix} \right] \tag{21}$$

Consequently, the control inputs of the USV are also differential functions of the flat outputs and the entire system is differentially flat. The differential flatness property of the USV can be used for defining setpoints for the system's state variables.

3 Approximate linearization of the USV state-space model

3.1 Approximately linearized dynamics of the USV

The dynamic model of the USV undergoes approximate linearization around the temporary operating point (x^*, u^*), where x^* is the present value of the USV's state vector and u^* is the last sampled value of the control inputs vector. The linearization relies on first-order Taylor series expansion and on the computation of the associated Jacobian matrices at each sampling instance. The initial nonlinear model of the USV

$$\dot{x} = f(x, u) \;\; \text{or} \quad \dot{x} = f(x) + g_1(x)u_1 + g_2(x)u_2 + g_3(x)u_3 \tag{22}$$

is substituted by its equivalent linearized description

$$\dot{x} = Ax + Bu + \tilde{d} \tag{23}$$

where $\tilde{d}$ is the cumulative disturbances vector. This may comprise (i) the modelling error due to truncation of higher-order terms in the Taylor series expansion, (ii) exogenous perturbations, (iii) sensor measurement noise of any distribution.

Matrices A and B are Jacobians of the linearization process and are given by

$$A = \nabla_x[f(x) + g_1(x)u_1 + g_2(x)u_2 + g_3(x)u_3] \mid_{(x^*,u^*)} \Rightarrow$$
$$A = \nabla_x f(x) \mid_{(x^*,u^*)} + \nabla_x g_1(x)u_1 \mid_{(x^*,u^*)} + \nabla_x g_2(x)u_2 \mid_{(x^*,u^*)} + \nabla_x g_3(x)u_3 \mid_{(x^*,u^*)} \tag{24}$$

$$B = \nabla_u[f(x) + g_1(x)u_1 + g_2(x)u_2 + g_3(x)u_3] \mid_{(x^*,u^*)} \Rightarrow$$
$$B = [g_1(x)\ g_2(x)\ g_3(x)] \mid_{(x^*,u^*)} \Rightarrow B = g(x) \mid_{(x^*,u^*)} \tag{25}$$

Computation of the Jacobian matrix $\nabla_x f(x) \mid_{(x^*,u^*)}$.

First row of the Jacobian matrix $\nabla_x f(x) \mid_{(x^*,u^*)}$: $\frac{\partial f_1}{\partial x_1} = 0$, $\frac{\partial f_1}{\partial x_2} = 1$, $\frac{\partial f_1}{\partial x_3} = 0$, $\frac{\partial f_1}{\partial x_4} = 0$, $\frac{\partial f_1}{\partial x_5} = 0$, and $\frac{\partial f_1}{\partial x_6} = 0$.

Second row of the Jacobian matrix $\nabla_x f(x) \mid_{(x^*,u^*)}$: for $i = 1, 2, \cdots, 6$

$$\frac{\partial f_2}{\partial x_i} = -\frac{[\frac{\partial J_{11}}{\partial x_i}(c_1 + q_1) + J_{11}(\frac{\partial c_1}{\partial x_i} + \frac{\partial q_1}{\partial x_i})]detJ - [J_{11}(c_1 + q_1)]\frac{\partial detJ}{\partial x_i}}{detJ^2} +$$
$$+ \frac{[\frac{\partial J_{21}}{\partial x_i}(c_2 + q_2) + J_{21}(\frac{\partial c_2}{\partial x_i} + \frac{\partial q_2}{\partial x_i})]detJ - [J_{21}(c_2 + q_2)]\frac{\partial detJ}{\partial x_i}}{detJ^2} -$$
$$- \frac{[\frac{\partial J_{31}}{\partial x_i}(c_3 + q_3) + J_{31}(\frac{\partial c_3}{\partial x_i} + \frac{\partial q_3}{\partial x_i})]detJ - [J_{31}(c_3 + q_3)]\frac{\partial detJ}{\partial x_i}}{detJ^2} \tag{26}$$

Third row of the Jacobian matrix $\nabla_x f(x) \mid_{(x^*,u^*)}$: $\frac{\partial f_3}{\partial x_1} = 0$, $\frac{\partial f_3}{\partial x_2} = 0$, $\frac{\partial f_3}{\partial x_3} = 0$, $\frac{\partial f_3}{\partial x_4} = 1$, $\frac{\partial f_3}{\partial x_5} = 0$, and $\frac{\partial f_3}{\partial x_6} = 0$.

Fourth row of the Jacobian matrix $\nabla_x f(x) \mid_{(x^*,u^*)}$: for $i = 1, 2, \cdots, 6$

$$\frac{\partial f_4}{\partial x_i} = \frac{[\frac{\partial J_{12}}{\partial x_i}(c_1 + q_1) + J_{12}(\frac{\partial c_1}{\partial x_i} + \frac{\partial q_1}{\partial x_i})]detJ - [J_{12}(c_1 + q_1)]\frac{\partial detJ}{\partial x_i}}{detJ^2} -$$
$$- \frac{[\frac{\partial J_{22}}{\partial x_i}(c_2 + q_2) + J_{22}(\frac{\partial c_2}{\partial x_i} + \frac{\partial q_2}{\partial x_i})]detJ - [J_{22}(c_2 + q_2)]\frac{\partial detJ}{\partial x_i}}{detJ^2} +$$
$$+ \frac{[\frac{\partial J_{32}}{\partial x_i}(c_3 + q_3) + J_{32}(\frac{\partial c_3}{\partial x_i} + \frac{\partial q_3}{\partial x_i})]detJ - [J_{32}(c_3 + q_3)]\frac{\partial detJ}{\partial x_i}}{detJ^2} \tag{27}$$

Fifth row of the Jacobian matrix $\nabla_x f(x) \mid_{(x^*,u^*)}$: $\frac{\partial f_5}{\partial x_1} = 0$, $\frac{\partial f_5}{\partial x_2} = 0$, $\frac{\partial f_5}{\partial x_3} = 0$, $\frac{\partial f_5}{\partial x_4} = 0$, $\frac{\partial f_5}{\partial x_5} = 0$, and $\frac{\partial f_5}{\partial x_6} = 1$.

Sixth row of the Jacobian matrix $\nabla_x f(x) \mid_{(x^*,u^*)}$: for $i = 1, 2, \cdots, 6$

$$\frac{\partial f_6}{\partial x_i} = -\frac{[\frac{\partial J_{13}}{\partial x_i}(c_1 + q_1) + J_{12}(\frac{\partial c_1}{\partial x_i} + \frac{\partial q_1}{\partial x_i})]detJ - [J_{13}(c_1 + q_1)]\frac{\partial detJ}{\partial x_i}}{detJ^2} +$$
$$+ \frac{[\frac{\partial J_{23}}{\partial x_i}(c_2 + q_2) + J_{23}(\frac{\partial c_2}{\partial x_i} + \frac{\partial q_2}{\partial x_i})]detJ - [J_{23}(c_2 + q_2)]\frac{\partial detJ}{\partial x_i}}{detJ^2} -$$
$$- \frac{[\frac{\partial J_{33}}{\partial x_i}(c_3 + q_3) + J_{33}(\frac{\partial c_3}{\partial x_i} + \frac{\partial q_3}{\partial x_i})]detJ - [J_{33}(c_3 + q_3)]\frac{\partial detJ}{\partial x_i}}{detJ^2} \tag{28}$$

Computation of the Jacobian matrix $\nabla_x g_1(x) \mid_{(x^*,u^*)}$.

First row of the Jacobian matrix $\nabla_x g_1(x) \mid_{(x^*,u^*)}$: $\frac{\partial g_{11}}{\partial x_i} = 0$, for $i = 1, 2, \cdots, 6$.

Second row of the Jacobian matrix $\nabla_x g_1(x) \mid_{(x^*,u^*)}$ for $i = 1, 2, \cdots, 6$

$$\frac{\partial g_{21}}{\partial x_i} = \frac{\frac{\partial J_{11}}{\partial x_i}detJ - J_{11}\frac{\partial detJ}{\partial x_i}}{detJ^2} \tag{29}$$

Third row of the Jacobian matrix $\nabla_x g_1(x) \mid_{(x^*,u^*)}$: $\frac{\partial g_{31}}{\partial x_i} = 0$, for $i = 1, 2, \cdots, 6$.

Fourth row of the Jacobian matrix $\nabla_x g_1(x) \mid_{(x^*,u^*)}$ for $i = 1, 2, \cdots, 6$

$$\frac{\partial g_{41}}{\partial x_i} = -\frac{\frac{\partial J_{12}}{\partial x_i}detJ - J_{12}\frac{\partial detJ}{\partial x_i}}{detJ^2} \tag{30}$$

Fifth row of the Jacobian matrix $\nabla_x g_1(x) \mid_{(x^*,u^*)}$: $\frac{\partial g_{51}}{\partial x_i} = 0$, for $i = 1, 2, \cdots, 6$.

Sixth row of the Jacobian matrix $\nabla_x g_1(x) \mid_{(x^*,u^*)}$ for $i = 1, 2, \cdots, 6$

$$\frac{\partial g_{61}}{\partial x_i} = \frac{\frac{\partial J_{13}}{\partial x_i}detJ - J_{13}\frac{\partial detJ}{\partial x_i}}{detJ^2} \tag{31}$$

Computation of the Jacobian matrix $\nabla_x g_2(x) \mid_{(x^*,u^*)}$.

First row of the Jacobian matrix $\nabla_x g_2(x) \mid_{(x^*,u^*)}$: $\frac{\partial g_{12}}{\partial x_i} = 0$, for $i = 1, 2, \cdots, 6$.

Second row of the Jacobian matrix $\nabla_x g_2(x) \mid_{(x^*,u^*)}$ for $i = 1, 2, \cdots, 6$

$$\frac{\partial g_{22}}{\partial x_i} = -\frac{\frac{\partial J_{21}}{\partial x_i}detJ - J_{21}\frac{\partial detJ}{\partial x_i}}{detJ^2} \tag{32}$$

Third row of the Jacobian matrix $\nabla_x g_2(x) \mid_{(x^*,u^*)}$: $\frac{\partial g_{32}}{\partial x_i} = 0$, for $i = 1, 2, \cdots, 6$.

Fourth row of the Jacobian matrix $\nabla_x g_2(x) \mid_{(x^*,u^*)}$ for $i = 1, 2, \cdots, 6$

$$\frac{\partial g_{42}}{\partial x_i} = \frac{\frac{\partial J_{22}}{\partial x_i}detJ - J_{22}\frac{\partial detJ}{\partial x_i}}{detJ^2} \tag{33}$$

Fifth row of the Jacobian matrix $\nabla_x g_2(x) \mid_{(x^*,u^*)}$: $\frac{\partial g_{52}}{\partial x_i} = 0$, for $i = 1, 2, \cdots, 6$.

Sixth row of the Jacobian matrix $\nabla_x g_2(x) \mid_{(x^*,u^*)}$ for $i = 1, 2, \cdots, 6$

$$\frac{\partial g_{62}}{\partial x_i} = -\frac{\frac{\partial J_{23}}{\partial x_i}detJ - J_{23}\frac{\partial detJ}{\partial x_i}}{detJ^2} \tag{34}$$

Computation of the Jacobian matrix $\nabla_x g_3(x) \mid_{(x^*,u^*)}$.

First row of the Jacobian matrix $\nabla_x g_3(x) \mid_{(x^*,u^*)}$: $\frac{\partial g_{13}}{\partial x_i} = 0$, for $i = 1, 2, \cdots, 6$.

Second row of the Jacobian matrix $\nabla_x g_3(x) \mid_{(x^*,u^*)}$ for $i = 1, 2, \cdots, 6$

$$\frac{\partial g_{23}}{\partial x_i} = \frac{\frac{\partial J_{31}}{\partial x_i}detJ - J_{31}\frac{\partial detJ}{\partial x_i}}{detJ^2} \tag{35}$$

Third row of the Jacobian matrix $\nabla_x g_3(x)\mid_{(x^*,u^*)}$: $\frac{\partial g_{33}}{\partial x_i}=0$, for $i=1,2,\cdots,6$.

Fourth row of the Jacobian matrix $\nabla_x g_3(x)\mid_{(x^*,u^*)}$ for $i=1,2,\cdots,6$

$$\frac{\partial g_{43}}{\partial x_i}=-\frac{\frac{\partial J_{32}}{\partial x_i}detJ-J_{32}\frac{\partial detJ}{\partial x_i}}{detJ^2} \tag{36}$$

Fifth row of the Jacobian matrix $\nabla_x g_3(x)\mid_{(x^*,u^*)}$: $\frac{\partial g_{53}}{\partial x_i}=0$, for $i=1,2,\cdots,6$.

Sixth row of the Jacobian matrix $\nabla_x g_3(x)\mid_{(x^*,u^*)}$ for $i=1,2,\cdots,6$

$$\frac{\partial g_{63}}{\partial x_i}=\frac{\frac{\partial J_{33}}{\partial x_i}detJ-J_{33}\frac{\partial detJ}{\partial x_i}}{detJ^2} \tag{37}$$

Next, the partial derivatives of the terms J_{ij} $i=1,2,3$, $j=1,2,3$ and of the determinant $detJ$ are computed. It holds that:

$$\frac{\partial J_{11}}{\partial x_i}=\frac{\partial \tilde{J}_{22}}{\partial x_i}\tilde{J}_{33}+\tilde{J}_{22}\frac{\partial \tilde{J}_{33}}{\partial x_i}-\frac{\partial \tilde{J}_{32}}{\partial x_i}\tilde{J}_{23}-\tilde{J}_{32}\frac{\partial \tilde{J}_{23}}{\partial x_i} \quad \text{for } i=1,2,\cdots,6 \tag{38}$$

$$\frac{\partial J_{12}}{\partial x_i}=\frac{\partial \tilde{J}_{21}}{\partial x_i}\tilde{J}_{33}+\tilde{J}_{21}\frac{\partial \tilde{J}_{33}}{\partial x_i}-\frac{\partial \tilde{J}_{31}}{\partial x_i}\tilde{J}_{23}-\tilde{J}_{31}\frac{\partial \tilde{J}_{23}}{\partial x_i} \quad \text{for } i=1,2,\cdots,6 \tag{39}$$

$$\frac{\partial J_{13}}{\partial x_i}=\frac{\partial \tilde{J}_{21}}{\partial x_i}\tilde{J}_{32}+\tilde{J}_{21}\frac{\partial \tilde{J}_{32}}{\partial x_i}-\frac{\partial \tilde{J}_{31}}{\partial x_i}\tilde{J}_{22}-\tilde{J}_{31}\frac{\partial \tilde{J}_{22}}{\partial x_i} \quad \text{for } i=1,2,\cdots,6 \tag{40}$$

$$\frac{\partial J_{21}}{\partial x_i}=\frac{\partial \tilde{J}_{12}}{\partial x_i}\tilde{J}_{33}+\tilde{J}_{12}\frac{\partial \tilde{J}_{33}}{\partial x_i}-\frac{\partial \tilde{J}_{32}}{\partial x_i}\tilde{J}_{13}-\tilde{J}_{32}\frac{\partial \tilde{J}_{13}}{\partial x_i} \quad \text{for } i=1,2,\cdots,6 \tag{41}$$

$$\frac{\partial J_{22}}{\partial x_i}=\frac{\partial \tilde{J}_{11}}{\partial x_i}\tilde{J}_{33}+\tilde{J}_{11}\frac{\partial \tilde{J}_{33}}{\partial x_i}-\frac{\partial \tilde{J}_{31}}{\partial x_i}\tilde{J}_{13}-\tilde{J}_{31}\frac{\partial \tilde{J}_{13}}{\partial x_i} \quad \text{for } i=1,2,\cdots,6 \tag{42}$$

$$\frac{\partial J_{23}}{\partial x_i}=\frac{\partial \tilde{J}_{11}}{\partial x_i}\tilde{J}_{32}+\tilde{J}_{11}\frac{\partial \tilde{J}_{32}}{\partial x_i}-\frac{\partial \tilde{J}_{31}}{\partial x_i}\tilde{J}_{12}-\tilde{J}_{31}\frac{\partial \tilde{J}_{12}}{\partial x_i} \quad \text{for } i=1,2,\cdots,6 \tag{43}$$

$$\frac{\partial J_{31}}{\partial x_i}=\frac{\partial \tilde{J}_{12}}{\partial x_i}\tilde{J}_{23}+\tilde{J}_{12}\frac{\partial \tilde{J}_{23}}{\partial x_i}-\frac{\partial \tilde{J}_{22}}{\partial x_i}\tilde{J}_{13}-\tilde{J}_{22}\frac{\partial \tilde{J}_{13}}{\partial x_i} \quad \text{for } i=1,2,\cdots,6 \tag{44}$$

$$\frac{\partial J_{32}}{\partial x_i}=\frac{\partial \tilde{J}_{11}}{\partial x_i}\tilde{J}_{23}+\tilde{J}_{11}\frac{\partial \tilde{J}_{23}}{\partial x_i}-\frac{\partial \tilde{J}_{21}}{\partial x_i}\tilde{J}_{13}-\tilde{J}_{21}\frac{\partial \tilde{J}_{13}}{\partial x_i} \quad \text{for } i=1,2,\cdots,6 \tag{45}$$

$$\frac{\partial J_{33}}{\partial x_i}=\frac{\partial \tilde{J}_{11}}{\partial x_i}\tilde{J}_{22}+\tilde{J}_{11}\frac{\partial \tilde{J}_{22}}{\partial x_i}-\frac{\partial \tilde{J}_{21}}{\partial x_i}\tilde{J}_{12}-\tilde{J}_{21}\frac{\partial \tilde{J}_{12}}{\partial x_i} \quad \text{for } i=1,2,\cdots,6 \tag{46}$$

Additionally, it holds that for $i=1,2.\cdots,6$

$$\begin{aligned}\frac{\partial detJ}{\partial x_i}&=\frac{\partial \tilde{J}_{11}}{\partial x_i}(\tilde{J}_{22}\tilde{J}_{33}-\tilde{J}_{32}\tilde{J}_{23})\\&+\tilde{J}_{11}(\frac{\partial \tilde{J}_{22}}{\partial x_i}\tilde{J}_{33}+\tilde{J}_{22}\frac{\partial \tilde{J}_{33}}{\partial x_i}-\frac{\partial \tilde{J}_{32}}{\partial x_i}\tilde{J}_{23}-\tilde{J}_{32}\frac{\partial \tilde{J}_{23}}{\partial x_i})+\\&\frac{\partial \tilde{J}_{12}}{\partial x_i}(\tilde{J}_{21}\tilde{J}_{33}-\tilde{J}_{31}\tilde{J}_{23})\\&+\tilde{J}_{12}(\frac{\partial \tilde{J}_{21}}{\partial x_i}\tilde{J}_{33}+\tilde{J}_{21}\frac{\partial \tilde{J}_{33}}{\partial x_i}-\frac{\partial \tilde{J}_{31}}{\partial x_i}\tilde{J}_{23}-\tilde{J}_{31}\frac{\partial \tilde{J}_{23}}{\partial x_i})+\\&\frac{\partial \tilde{J}_{13}}{\partial x_i}(\tilde{J}_{21}\tilde{J}_{32}-\tilde{J}_{31}\tilde{J}_{22})\\&+\tilde{J}_{13}(\frac{\partial \tilde{J}_{21}}{\partial x_i}\tilde{J}_{32}+\tilde{J}_{21}\frac{\partial \tilde{J}_{32}}{\partial x_i}-\frac{\partial \tilde{J}_{31}}{\partial x_i}\tilde{J}_{22}-\tilde{J}_{31}\frac{\partial \tilde{J}_{22}}{\partial x_i})+\end{aligned} \tag{47}$$

Equivalently, one has for the partial derivatives of c_i, $i=1,2,3$

$$\begin{aligned}\frac{\partial c_1}{\partial x_i}&=\frac{\partial \tilde{C}_{11}}{\partial x_i}\dot{\eta}_1+\tilde{C}_{11}\frac{\partial \dot{\eta}_1}{\partial x_i}+\frac{\partial \tilde{C}_{12}}{\partial x_i}\dot{\eta}_2+\tilde{C}_{12}\frac{\partial \dot{\eta}_2}{\partial x_i}\\&+\frac{\partial \tilde{C}_{13}}{\partial x_i}\dot{\eta}_3+\tilde{C}_{13}\frac{\partial \dot{\eta}_3}{\partial x_i}\ \text{ for } i=1,2\cdots,6\end{aligned} \tag{48}$$

$$\begin{aligned}\frac{\partial c_2}{\partial x_i}&=\frac{\partial \tilde{C}_{21}}{\partial x_i}\dot{\eta}_1+\tilde{C}_{21}\frac{\partial \dot{\eta}_1}{\partial x_i}+\frac{\partial \tilde{C}_{22}}{\partial x_i}\dot{\eta}_2+\tilde{C}_{22}\frac{\partial \dot{\eta}_2}{\partial x_i}\\&+\frac{\partial \tilde{C}_{23}}{\partial x_i}\dot{\eta}_3+\tilde{C}_{23}\frac{\partial \dot{\eta}_3}{\partial x_i}\ \text{ for } i=1,2\cdots,6\end{aligned} \tag{49}$$

$$\begin{aligned}\frac{\partial c_3}{\partial x_i}&=\frac{\partial \tilde{C}_{31}}{\partial x_i}\dot{\eta}_1+\tilde{C}_{31}\frac{\partial \dot{\eta}_1}{\partial x_i}+\frac{\partial \tilde{C}_{32}}{\partial x_i}\dot{\eta}_2+\tilde{C}_{32}\frac{\partial \dot{\eta}_2}{\partial x_i}\\&+\frac{\partial \tilde{C}_{33}}{\partial x_i}\dot{\eta}_3+\tilde{C}_{33}\frac{\partial \dot{\eta}_3}{\partial x_i}\ \text{ for } i=1,2\cdots,6\end{aligned} \tag{50}$$

Additionally, one has for the partial derivatives of c_i, $i=1,2,3$

$$\begin{aligned}\frac{\partial q_1}{\partial x_i}&=\frac{\partial \tilde{F}_{11}}{\partial x_i}\dot{\eta}_1+\tilde{F}_{11}\frac{\partial \dot{\eta}_1}{\partial x_i}+\frac{\partial \tilde{F}_{12}}{\partial x_i}\dot{\eta}_2+\tilde{F}_{12}\frac{\partial \dot{\eta}_2}{\partial x_i}\\&+\frac{\partial \tilde{F}_{13}}{\partial x_i}\dot{\eta}_3+\tilde{F}_{13}\frac{\partial \dot{\eta}_3}{\partial x_i}\ \text{ for } i=1,2\cdots,6\end{aligned} \tag{51}$$

$$\frac{\partial q_2}{\partial x_i} = \frac{\partial \tilde{F}_{21}}{\partial x_i}\dot{\eta}_1 + \tilde{F}_{21}\frac{\partial \dot{\eta}_1}{\partial x_i} + \frac{\partial \tilde{F}_{22}}{\partial x_i}\dot{\eta}_2 + \tilde{F}_{22}\frac{\partial \dot{\eta}_2}{\partial x_i} + \frac{\partial \tilde{F}_{23}}{\partial x_i}\dot{\eta}_3 + \tilde{F}_{23}\frac{\partial \dot{\eta}_3}{\partial x_i} \quad \text{for } i = 1, 2 \cdots, 6 \tag{52}$$

$$\frac{\partial q_3}{\partial x_i} = \frac{\partial \tilde{F}_{31}}{\partial x_i}\dot{\eta}_1 + \tilde{F}_{31}\frac{\partial \dot{\eta}_1}{\partial x_i} + \frac{\partial \tilde{F}_{32}}{\partial x_i}\dot{\eta}_2 + \tilde{F}_{32}\frac{\partial \dot{\eta}_2}{\partial x_i} + \frac{\partial \tilde{F}_{33}}{\partial x_i}\dot{\eta}_3 + \tilde{F}_{33}\frac{\partial \dot{\eta}_3}{\partial x_i} \quad \text{for } i = 1, 2 \cdots, 6 \tag{53}$$

Moreover, about the partial derivatives of variables η_i, $i = 1, 2, 3$ one has that

$$\frac{\partial \dot{\eta}_1}{\partial x_2} = 1 \quad \frac{\partial \dot{\eta}_1}{\partial x_i} = 0 \ \text{ for } i = 1, 3, 4, 5, 6 \tag{54}$$

$$\frac{\partial \dot{\eta}_2}{\partial x_4} = 1 \quad \frac{\partial \dot{\eta}_2}{\partial x_i} = 0 \ \text{ for } i = 1, 2, 3, 5, 6 \tag{55}$$

$$\frac{\partial \dot{\eta}_3}{\partial x_6} = 1 \quad \frac{\partial \dot{\eta}_3}{\partial x_i} = 0 \ \text{ for } i = 1, 2, 3, 4, 5 \tag{56}$$

Next, one proceeds to the computation of the partial derivatives $\frac{\partial \tilde{J}_{ij}}{\partial x_i}$ $i = 1, 2, 3,$ $j = 1, 2, 3,$ $\frac{\partial \tilde{C}_{ij}}{\partial x_i}$ $i = 1, 2, 3,$ $j = 1, 2, 3$ and $\frac{\partial \tilde{F}_{ij}}{\partial x_i}$ $i = 1, 2, 3,$ $j = 1, 2, 3$. It holds that:

$$\frac{\partial \tilde{J}_{11}}{\partial x_i} = 0 \text{ for } i = 1, 2, 3, 4, 6 \text{ and } \frac{\partial \tilde{J}_{11}}{\partial x_5} = -2m_{11}cos(x_5)sin(x_5) + 2m_{22}sin(x_5)cos(x_5).$$

$$\frac{\partial \tilde{J}_{12}}{\partial x_i} = 0 \text{ for } i = 1, 2, 3, 4, 6 \text{ and } \frac{\partial \tilde{J}_{12}}{\partial x_5} = (m_{11} - m_{22})[cos^2(x_5) - sin^2(x_5)].$$

$$\frac{\partial \tilde{J}_{13}}{\partial x_i} = 0 \text{ for } i = 1, 2, 3, 4, 6 \text{ and } \frac{\partial \tilde{J}_{13}}{\partial x_5} = -m_{23}cos(x_5).$$

$$\frac{\partial \tilde{J}_{21}}{\partial x_i} = 0 \text{ for } i = 1, 2, 3, 4, 6 \text{ and } \frac{\partial \tilde{J}_{21}}{\partial x_5} = -(m_{11} - m_{22})[cos^2(x_5) - sin^2(x_5)].$$

$$\frac{\partial \tilde{J}_{22}}{\partial x_i} = 0 \text{ for } i = 1, 2, 3, 4, 6 \text{ and } \frac{\partial \tilde{J}_{22}}{\partial x_5} = 2m_{11}sin(x_5)cos(x_5) - 2m_{22}sin(x_5)cos(x_5).$$

$$\frac{\partial \tilde{J}_{23}}{\partial x_i} = 0 \text{ for } i = 1, 2, 3, 4, 6 \text{ and } \frac{\partial \tilde{J}_{23}}{\partial x_5} = -m_{23}sin(x_5).$$

$$\frac{\partial \tilde{J}_{31}}{\partial x_i} = 0 \text{ for } i = 1, 2, 3, 4, 6 \text{ and } \frac{\partial \tilde{J}_{31}}{\partial x_5} = -m_{23}cos(x_5).$$

$$\frac{\partial \tilde{J}_{32}}{\partial x_i} = 0 \text{ for } i = 1, 2, 3, 4, 6 \text{ and } \frac{\partial \tilde{J}_{32}}{\partial x_5} = -m_{23}cos(x_5).$$

$$\frac{\partial \tilde{J}_{33}}{\partial x_i} = 0 \text{ for } i = 1, 2, 3, 4, 4, 6$$

Furthermore, it holds that

$$\frac{\partial \tilde{F}_{11}}{\partial x_i} = 0 \text{ for } i = 1,2,3,4,6 \text{ and } \frac{\partial \tilde{F}_{11}}{\partial x_5} = -2d_{11}cos(x_5)sin(x_5) + 2d_{22}sin(x_5)cos(x_5).$$

$$\frac{\partial \tilde{F}_{12}}{\partial x_i} = 0 \text{ for } i = 1,2,3,4,6 \text{ and } \frac{\partial \tilde{F}_{12}}{\partial x_5} = (d_{11} - d_{22})[cos^2(x_5) - sin^2(x_5)].$$

$$\frac{\partial \tilde{F}_{13}}{\partial x_i} = 0 \text{ for } i = 1,2,3,4,6 \text{ and } \frac{\partial \tilde{F}_{13}}{\partial x_5} = -d_{23}cos(x_5).$$

$$\frac{\partial \tilde{F}_{21}}{\partial x_i} = 0 \text{ for } i = 1,2,3,4,6 \text{ and } \frac{\partial \tilde{F}_{21}}{\partial x_5} = (d_{11} - d_{22})[cos^2(x_5) - sin^2(x_5)].$$

$$\frac{\partial \tilde{F}_{22}}{\partial x_i} = 0 \text{ for } i = 1,2,3,4,6 \text{ and } \frac{\partial \tilde{F}_{22}}{\partial x_5} = 2d_{11}sin(x_5)cos(x_5) - 2d_{22}sin(x_5)cos(x_5).$$

$$\frac{\partial \tilde{F}_{23}}{\partial x_i} = 0 \text{ for } i = 1,2,3,4,6 \text{ and } \frac{\partial \tilde{F}_{23}}{\partial x_5} = -d_{22}sin(x_5).$$

$$\frac{\partial \tilde{F}_{31}}{\partial x_i} = 0 \text{ for } i = 1,2,3,4,6 \text{ and } \frac{\partial \tilde{F}_{31}}{\partial x_5} = -d_{32}cos(x_5).$$

$$\frac{\partial \tilde{F}_{32}}{\partial x_i} = 0 \text{ for } i = 1,2,3,4,6 \text{ and } \frac{\partial \tilde{F}_{32}}{\partial x_5} = -d_{32}sin(x_5).$$

$$\frac{\partial \tilde{F}_{33}}{\partial x_i} = 0 \text{ for } i = 1,2,3,4,5,6.$$

3.2 Stabilizing feedback control

After linearization around its current operating point (x^*, u^*), the dynamic model of the Unmanned Surface Vessel (USV) is written as [1]

$$\dot{x} = Ax + Bu + d_1 \tag{57}$$

Parameter d_1 stands for the linearization error in the USV's model appearing previously in Eq. (57). The reference setpoints for the USV's state vector are denoted by $\mathbf{x_d} = [x_1^d, \cdots, x_6^d]$. Tracking of this trajectory is achieved after applying the control input u^*. At every time instant the control input u^* is assumed to differ from the control input u appearing in Eq. (57) by an amount equal to Δu, that is $u^* = u + \Delta u$

$$\dot{x}_d = Ax_d + Bu^* + d_2 \tag{58}$$

The dynamics of the controlled system described in Eq. (57) can be also written as

$$\dot{x} = Ax + Bu + Bu^* - Bu^* + d_1 \tag{59}$$

and by denoting $d_3 = -Bu^* + d_1$ as an aggregate disturbance term one obtains

$$\dot{x} = Ax + Bu + Bu^* + d_3 \tag{60}$$

By subtracting Eq. (58) from Eq. (60) one has

$$\dot{x} - \dot{x}_d = A(x - x_d) + Bu + d_3 - d_2 \tag{61}$$

By denoting the tracking error as $e = x - x_d$ and the aggregate disturbance term as $L{\cdot}\tilde{d} = d_3 - d_2$, the tracking error dynamics becomes

$$\dot{e} = Ae + Bu + L\tilde{d} \tag{62}$$

where L is the disturbance inputs gain matrix. For the approximately linearized model of the system a stabilizing feedback controller is developed. The controller has the form

$$u(t) = -Ke(t) \tag{63}$$

with $K = \frac{1}{r}B^TP$ where P is a positive definite symmetric matrix which is obtained from the solution of the Riccati equation [1]

$$A^TP + PA + Q - P(\frac{2}{r}BB^T - \frac{1}{\rho^2}LL^T)P = 0 \tag{64}$$

where Q is a positive semi-definite symmetric matrix. The diagram of the considered control loop for the USV is depicted in Fig. 2.

4 Lyapunov stability analysis

4.1 Stability proof

Through Lyapunov stability analysis it will be shown that the proposed nonlinear control scheme assures H_∞ tracking performance for the Unmanned Surface Vessel (USV), and that in case of bounded disturbance terms asymptotic convergence to the reference setpoints is achieved [1, 37]. The tracking error dynamics for the USV is written in the form

$$\dot{e} = Ae + Bu + L\tilde{d} \tag{65}$$

where in the 3-DOF USV's case $L = I \in R^6$ with I being the identity matrix. Variable $\tilde{d}$ denotes model uncertainties and external disturbances of the USV's model. The following Lyapunov equation is considered

$$V = \frac{1}{2}e^TPe \tag{66}$$

where $e = x - x_d$ is the tracking error. By differentiating with respect to time one obtains

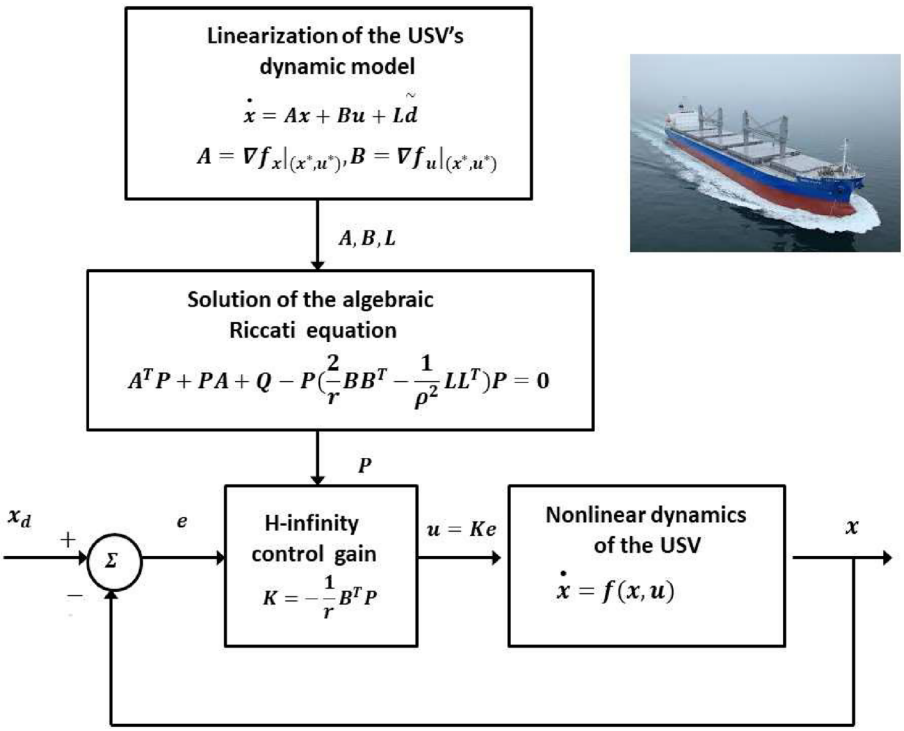

Fig. 2 Diagram of the control scheme for the Unmanned Surface Vessel

$$\dot{V} = \frac{1}{2}\dot{e}^T Pe + \frac{1}{2}e^T P\dot{e} \Rightarrow$$
$$\dot{V} = \frac{1}{2}[Ae + Bu + L\tilde{d}]^T Pe + \frac{1}{2}e^T P[Ae + Bu + L\tilde{d}] \Rightarrow \quad (67)$$

$$\dot{V} = \frac{1}{2}[e^TA^T + u^TB^T + \tilde{d}^TL^T]Pe + \frac{1}{2}e^TP[Ae + Bu + L\tilde{d}] \Rightarrow \quad (68)$$

$$\dot{V} = \frac{1}{2}e^TA^TPe + \frac{1}{2}u^TB^TPe + \frac{1}{2}\tilde{d}^TL^TPe + \frac{1}{2}e^TPAe + \frac{1}{2}e^TPBu + \frac{1}{2}e^TPL\tilde{d} \quad (69)$$

The previous equation is rewritten as

$$\dot{V} = \frac{1}{2}e^T(A^TP + PA)e + (\frac{1}{2}u^TB^TPe + \frac{1}{2}e^TPBu) + (\frac{1}{2}\tilde{d}^TL^TPe + \frac{1}{2}e^TPL\tilde{d}) \quad (70)$$

Assumption: For given positive definite matrix Q and coefficients r and ρ there exists a positive definite matrix P, which is the solution of the following matrix equation

$$A^TP + PA = -Q + P(\frac{2}{r}BB^T - \frac{1}{\rho^2}LL^T)P \quad (71)$$

Moreover, the following feedback control law is applied to the system

$$u = -\frac{1}{r}B^TPe \quad (72)$$

By substituting Eq. (71) and Eq. (72) one obtains

$$\dot{V} = \frac{1}{2}e^T[-Q + P(\frac{2}{r}BB^T - \frac{1}{\rho^2}LL^T)P]e + e^TPB(-\frac{1}{r}B^TPe) + e^TPL\tilde{d} \Rightarrow \quad (73)$$

$$\dot{V} = -\frac{1}{2}e^TQe + \frac{1}{r}e^TPBB^TPe - \frac{1}{2\rho^2}e^TPLL^TPe - \frac{1}{r}e^TPBB^TPe + e^TPL\tilde{d} \quad (74)$$

which after intermediate operations gives

$$\dot{V} = -\frac{1}{2}e^TQe - \frac{1}{2\rho^2}e^TPLL^TPe + e^TPL\tilde{d} \quad (75)$$

or, equivalently

$$\dot{V} = -\frac{1}{2}e^T Qe - \frac{1}{2\rho^2}e^T PLL^T Pe + \\ + \frac{1}{2}e^T PL\tilde{d} + \frac{1}{2}\tilde{d}^T L^T Pe \tag{76}$$

Lemma : *The following inequality holds*

$$\frac{1}{2}e^T L\tilde{d} + \frac{1}{2}\tilde{d}L^T Pe - \frac{1}{2\rho^2}e^T PLL^T Pe \leq \frac{1}{2}\rho^2\tilde{d}^T\tilde{d} \tag{77}$$

Proof : The binomial $(\rho\alpha - \frac{1}{\rho}b)^2$ is considered. Expanding the left part of the above inequality one gets

$$\rho^2 a^2 + \frac{1}{\rho^2}b^2 - 2ab \geq 0 \Rightarrow \frac{1}{2}\rho^2 a^2 + \frac{1}{2\rho^2}b^2 - ab \geq 0 \Rightarrow \\ ab - \frac{1}{2\rho^2}b^2 \leq \frac{1}{2}\rho^2 a^2 \Rightarrow \frac{1}{2}ab + \frac{1}{2}ab - \frac{1}{2\rho^2}b^2 \leq \frac{1}{2}\rho^2 a^2 \tag{78}$$

The following substitutions are carried out: $a = \tilde{d}$ and $b = e^T PL$ and the previous relation becomes

$$\frac{1}{2}\tilde{d}^T L^T Pe + \frac{1}{2}e^T PL\tilde{d} - \frac{1}{2\rho^2}e^T PLL^T Pe \leq \frac{1}{2}\rho^2\tilde{d}^T\tilde{d} \tag{79}$$

Eq. (79) is substituted in Eq. (76) and the inequality is enforced, thus giving

$$\dot{V} \leq -\frac{1}{2}e^T Qe + \frac{1}{2}\rho^2\tilde{d}^T\tilde{d} \tag{80}$$

Eq. (80) shows that the H_∞ tracking performance criterion is satisfied. The integration of $\dot{V}$ from 0 to T gives

$$\int_0^T \dot{V}(t)dt \leq -\frac{1}{2}\int_0^T ||e||_Q^2 dt + \frac{1}{2}\rho^2\int_0^T ||\tilde{d}||^2 dt \Rightarrow \\ 2V(T) + \int_0^T ||e||_Q^2 dt \leq 2V(0) + \rho^2\int_0^T ||\tilde{d}||^2 dt \tag{81}$$

Moreover, if there exists a positive constant $M_d > 0$ such that

$$\int_0^\infty ||\tilde{d}||^2 dt \leq M_d \tag{82}$$

then one gets

$$\int_0^\infty ||e||_Q^2 dt \leq 2V(0) + \rho^2 M_d \tag{83}$$

Thus, the integral $\int_0^\infty ||e||_Q^2 dt$ is bounded. Moreover, $V(T)$ is bounded and from the definition of the Lyapunov function V in Eq. (66) it becomes clear that $e(t)$ will be also bounded since $e(t) \in \Omega_e = \{e | e^T Pe \leq 2V(0) + \rho^2 M_d\}$. According to the above and with the use of Barbalat's Lemma one obtains $\lim_{t\to\infty} e(t) = 0$.

The outline of the global stability proof is that at each iteration of the control algorithm the state vector of the fully actuated USV converges towards the temporary operating point and the temporary operating point in turn converges towards the reference trajectory. Thus, the control scheme exhibits global asymptotic stability properties and not local stability. Assume the i-th iteration of the control algorithm and the i-th time interval about which a positive definite symmetric matrix P is obtained from the solution of the Riccati Equation appearing in Eq. (71). By following the stages of the stability proof one arrives at Eq. (80) which shows that the H-infinity tracking performance criterion holds. By selecting the attenuation coefficient ρ to be sufficiently small and in particular to satisfy $\rho^2 < ||e||_Q^2 / ||\tilde{d}||^2$ one has that the first derivative of the Lyapunov function is upper bounded by 0. Therefore for the i-th time interval it is proven that the Lyapunov function defined in Eq (66) is a decreasing one. This signifies that between the beginning and the end of the i-th time interval there will be a drop of the value of the Lyapunov function and since matrix P is a positive definite one, the only way for this to happen is the Euclidean norm of the state vector error e to be decreasing. This means that comparing to the beginning of each time interval, the distance of the state vector error from 0 at the end of the time interval has diminished. Consequently as the iterations of the control algorithm advance the tracking error will approach zero, and this is a global asymptotic stability condition.

4.1.1 Robust state estimation with Kalman filtering

The control loop has to be implemented with the use of information provided by a small number of sensors and by processing only a small number of state variables. To reconstruct the missing information about the state vector of the Unmanned Surface Vessel (USV) it is proposed to use a filtering scheme and based on it to apply state estimation-based control [1, 37]. By denoting as $A(k)$, $B(k)$ and $C(k)$ the discrete-time equivalents of matrices A, B and C of the linearized state-space model of the system, the recursion of the H_∞ Kalman Filter, for the 3-DOF USV, can be formulated in terms of a *measurement update* and a *time update* part

Measurement update:

$$D(k) = [I - \theta W(k)P^-(k) + C^T(k)R(k)^{-1}C(k)P^-(k)]^{-1} \\ K(k) = P^-(k)D(k)C^T(k)R(k)^{-1} \\ \hat{x}(k) = \hat{x}^-(k) + K(k)[y(k) - C\hat{x}^-(k)] \tag{84}$$

Time update:

$$\begin{aligned} \hat{x}^{-}(k+1) &= A(k)x(k) + B(k)u(k) \\ P^{-}(k+1) &= A(k)P^{-}(k)D(k)A^{T}(k) + Q(k) \end{aligned} \tag{85}$$

where it is assumed that parameter θ is sufficiently small to assure that the covariance matrix $P^{-}(k)^{-1} - \theta W(k) + C^{T}(k)R(k)^{-1}C(k)$ will be positive definite. When $\theta = 0$ the H_{∞} Kalman Filter becomes equivalent to the standard Kalman Filter. One can measure only a part of the state vector of the 3-DOF USV, for instance state variables x_1 (position of x-axis), x_2 (position on the y-axis), x_5 (heading angle of the USV) and x_6 (rate of change of heading angle), and can estimate through filtering the rest of the state vector elements. Moreover, the proposed Kalman filtering method can be used for sensor fusion purposes.

5 Simulation tests

The performance of the proposed nonlinear optimal control scheme for the USV is further confirmed through simulation experiments. The model of the unmanned surface vessel that has been considered in these tests is the one which has been used in [3]. Certainly, the results can be generalized for underactuated USVs. The sampling period was $T_s = 0.01$ sec. To compute the control inputs of the USV, the algebraic Riccati equation of Eq. (71) had to be solved at each time-step of the control algorithm. The tracking performance of the control scheme was tested using several reference paths that the USV had to follow. The obtained results are depicted in Figs. 3, 4, 5, 6, 7, 8, 9, 10, 11, 12, 13, 14, 15, 16, 17 and 18. The real values of the USV's state vector are printed in blue, the estimated values which were provided by the H-infinity Kalman Filter are plotted in green, while

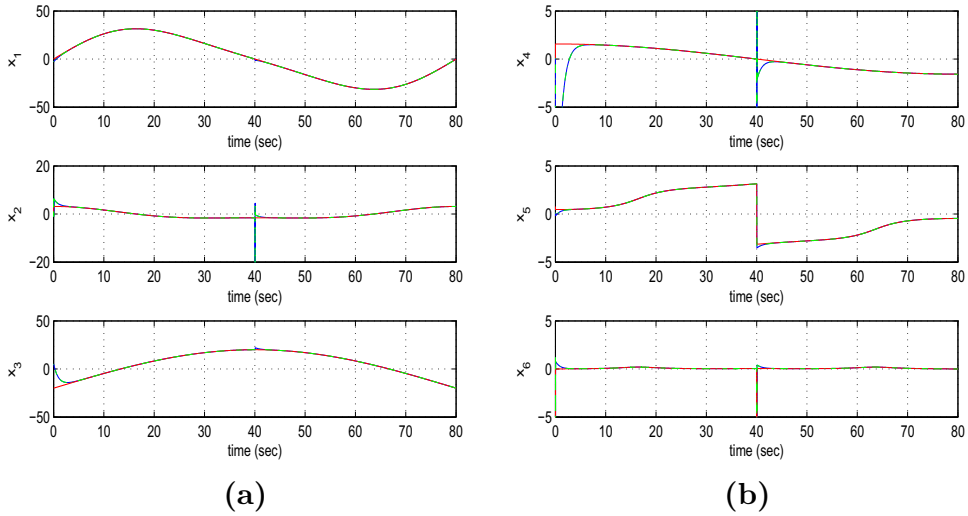

Fig. 3 Tracking of setpoint 1 for the 3-DOF USV **a** convergence of state variables x_1 to x_3 to their reference setpoints (red line: setpoint, blue line: real value, green line: estimated value), **b** convergence of state variables x_4 to x_6 to their reference setpoints (red line: setpoint, blue line: real value, green line: estimated value)

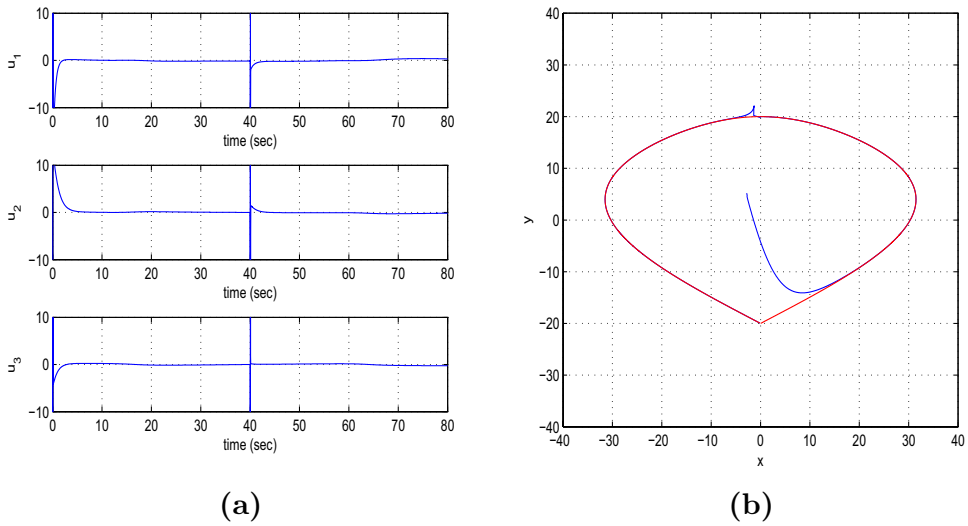

Fig. 4 Tracking of setpoint 1 for the 3-DOF USV **a** control inputs u_1 to u_3 applied to the propulsion and steering system of the USV, **b** tracking of the reference path (red line) by the USV (blue line) in the xy plane

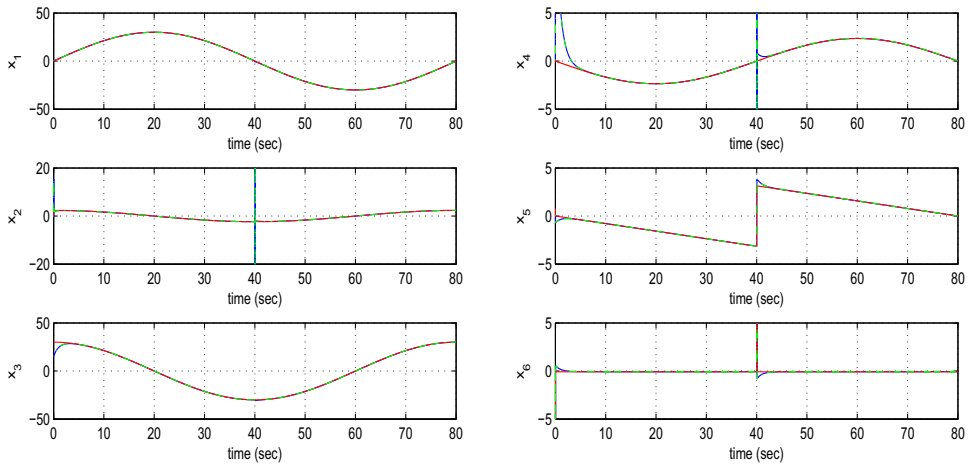

Fig. 5 Tracking of setpoint 2 for the 3-DOF USV **a** convergence of state variables x_1 to x_3 to their reference setpoints (red line: setpoint, blue line: real value, green line: estimated value), **b** convergence of state variables x_4 to x_6 to their reference setpoints (red line: setpoint, blue line: real value, green line: estimated value)

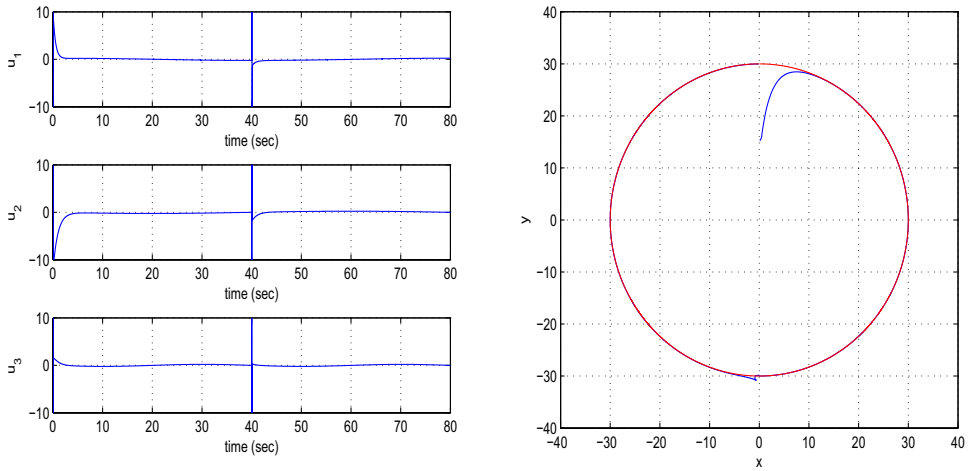

Fig. 6 Tracking of setpoint 2 for the 3-DOF USV **a** control inputs u_1 to u_3 applied to the propulsion and steering system of the USV, **b** tracking of the reference path (red line) by the USV (blue line) in the xy plane

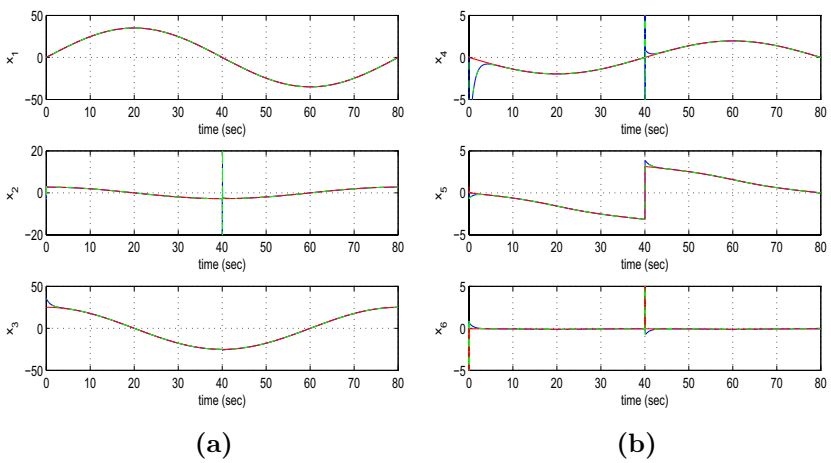

Fig. 7 Tracking of setpoint 3 for the 3-DOF USV **a** convergence of state variables x_1 to x_3 to their reference setpoints (red line: setpoint, blue line: real value, green line: estimated value), **b** convergence of state variables x_4 to x_6 to their reference setpoints (red line: setpoint, blue line: real value, green line: estimated value)

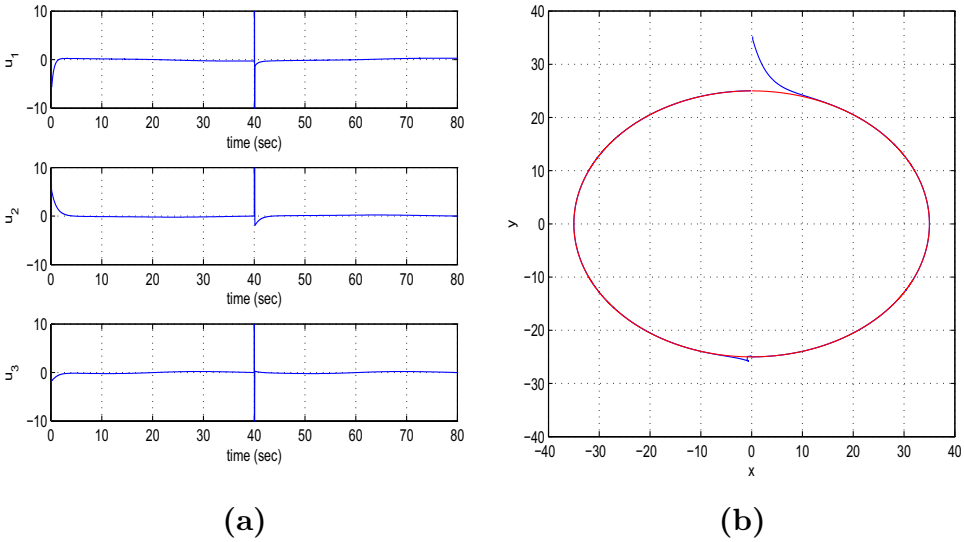

Fig. 8 Tracking of setpoint 3 for the 3-DOF USV **a** control inputs u_1 to u_3 applied to the propulsion and steering system of the USV, **b** tracking of the reference path (red line) by the USV (blue line) in the xy plane

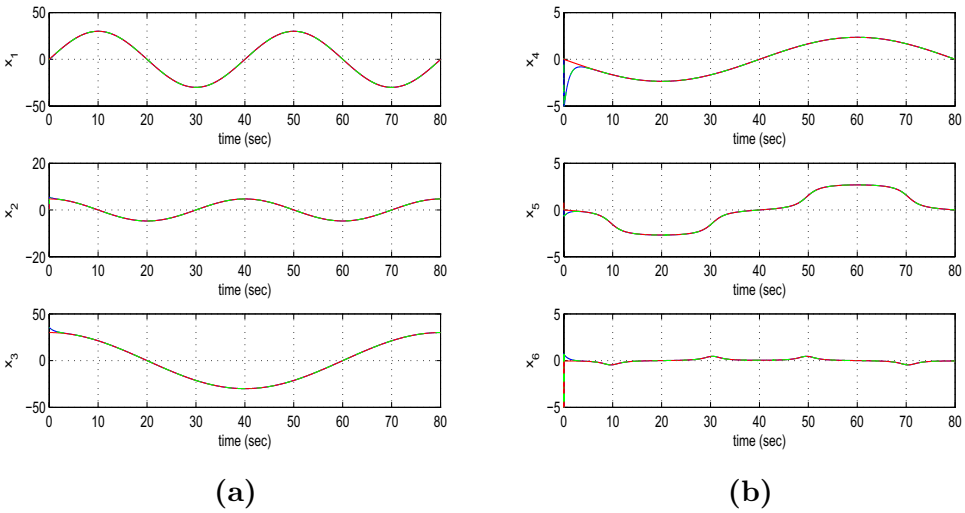

Fig. 9 Tracking of setpoint 4 for the 3-DOF USV **a** convergence of state variables x_1 to x_3 to their reference setpoints (red line: setpoint, blue line: real value, green line: estimated value), **b** convergence of state variables x_4 to x_6 to their reference setpoints (red line: setpoint, blue line: real value, green line: estimated value)

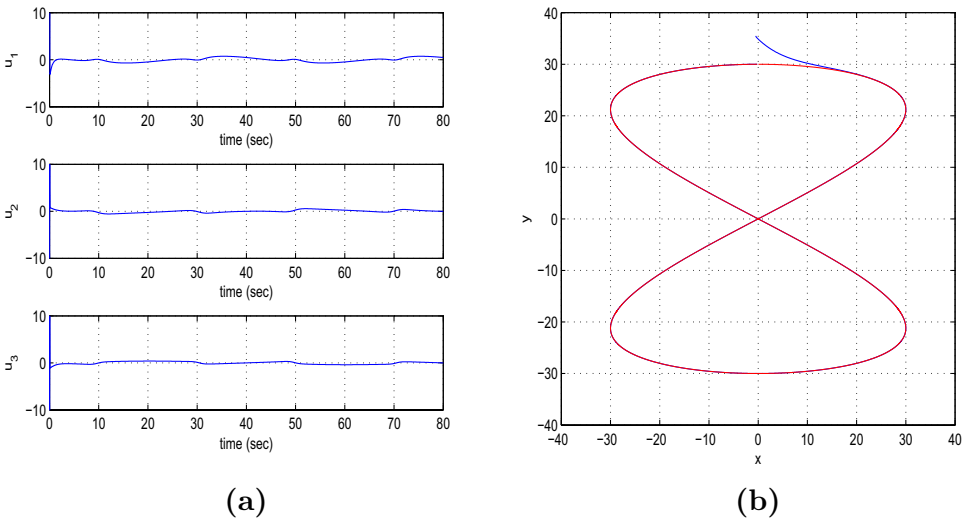

Fig. 10 Tracking of setpoint 4 for the 3-DOF USV **a** control inputs u_1 to u_3 applied to the propulsion and steering system of the USV, **b** tracking of the reference path (red line) by the USV (blue line) in the xy plane

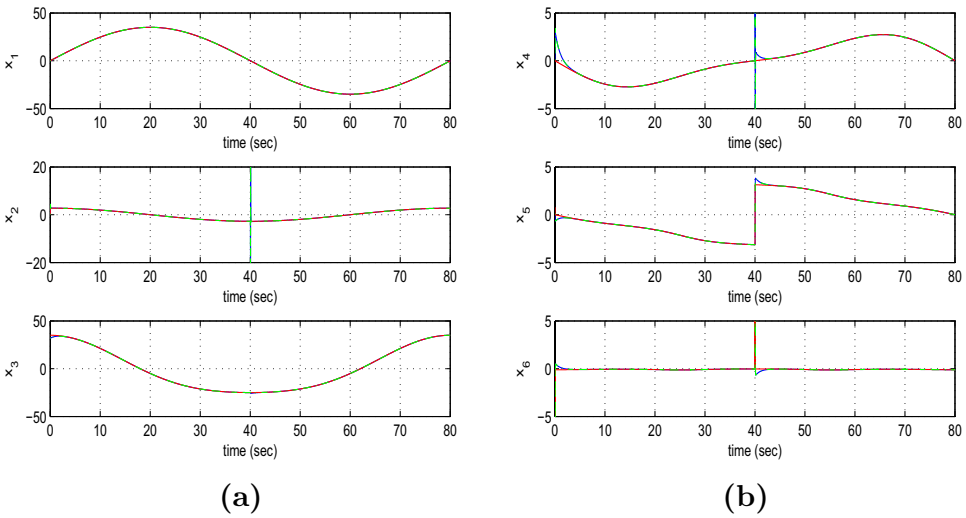

Fig. 11 Tracking of setpoint 5 for the 3-DOF USV **a** convergence of state variables x_1 to x_3 to their reference setpoints (red line: setpoint, blue line: real value, green line: estimated value), **b** convergence of state variables x_4 to x_6 to their reference setpoints (red line: setpoint, blue line: real value, green line: estimated value)

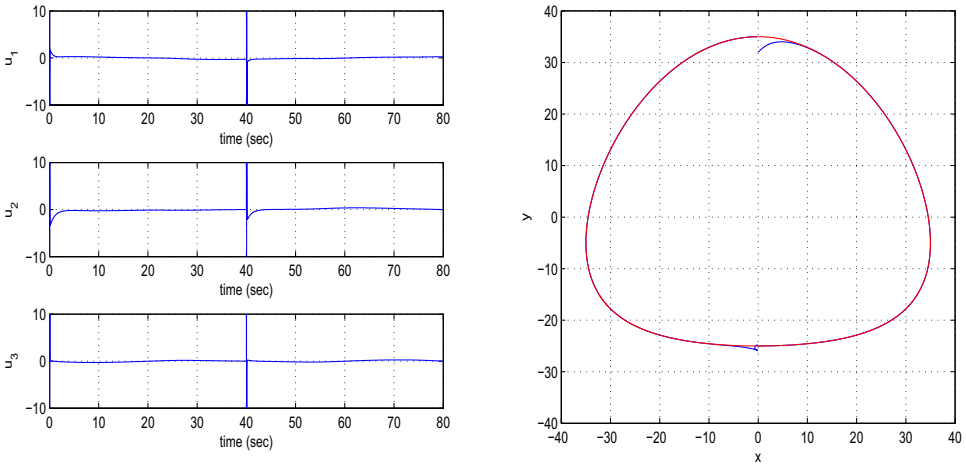

Fig. 12 Tracking of setpoint 5 for the 3-DOF USV **a** control inputs u_1 to u_3 applied to the propulsion and steering system of the USV, **b** tracking of the reference path (red line) by the USV (blue line) in the xy plane

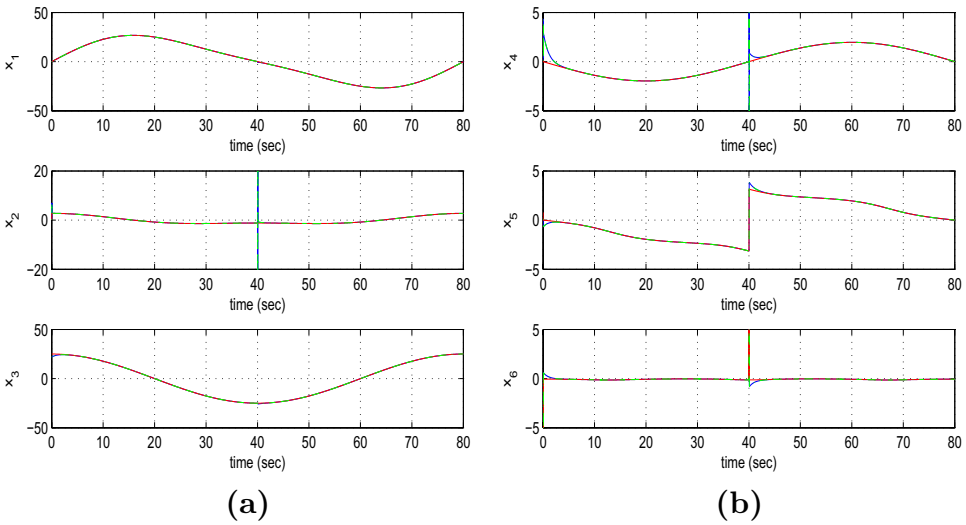

Fig. 13 Tracking of setpoint 6 for the 3-DOF USV **a** convergence of state variables x_1 to x_3 to their reference setpoints (red line: setpoint, blue line: real value, green line: estimated value), **b** convergence of state variables x_4 to x_6 to their reference setpoints (red line: setpoint, blue line: real value, green line: estimated value)

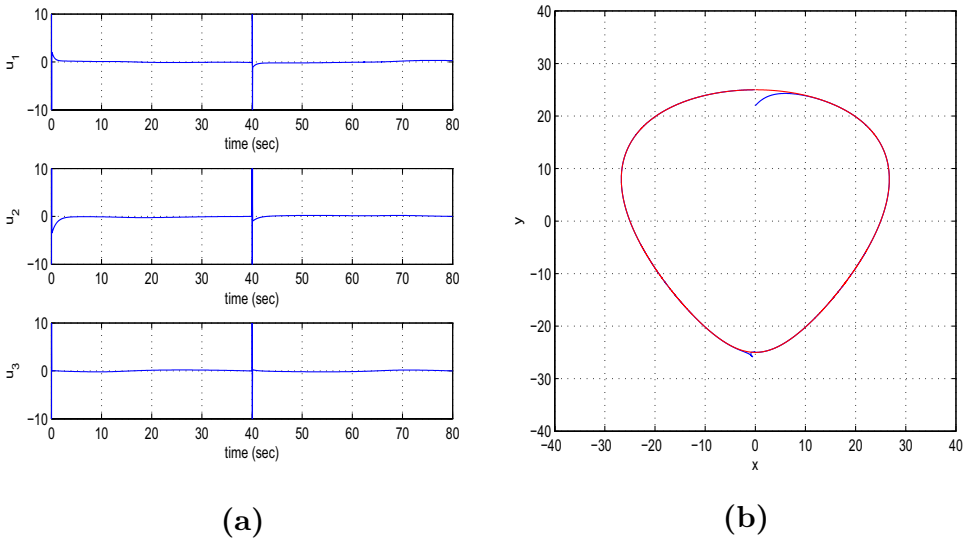

Fig. 14 Tracking of setpoint 6 for the 3-DOF USV **a** control inputs u_1 to u_3 applied to the propulsion and steering system of the USV, **b** tracking of the reference path (red line) by the USV (blue line) in the *xy* plane

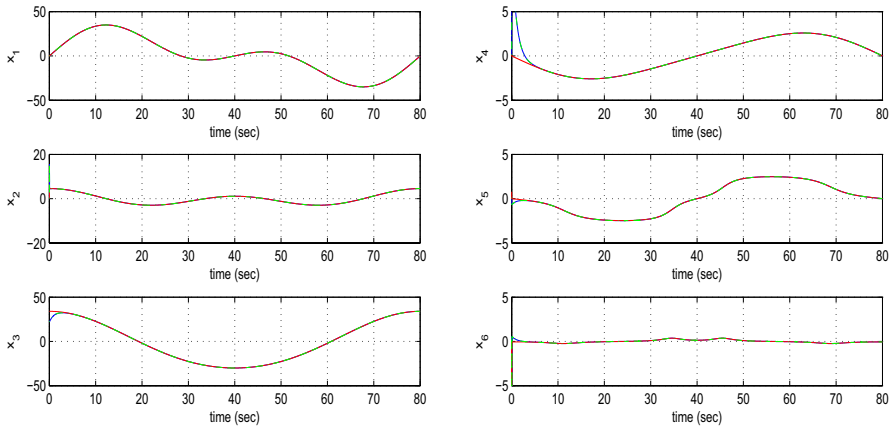

Fig. 15 Tracking of setpoint 7 for the 3-DOF USV **a** convergence of state variables x_1 to x_3 to their reference setpoints (red line: setpoint, blue line: real value, green line: estimated value), **b** convergence of state variables x_4 to x_6 to their reference setpoints (red line: setpoint, blue line: real value, green line: estimated value)

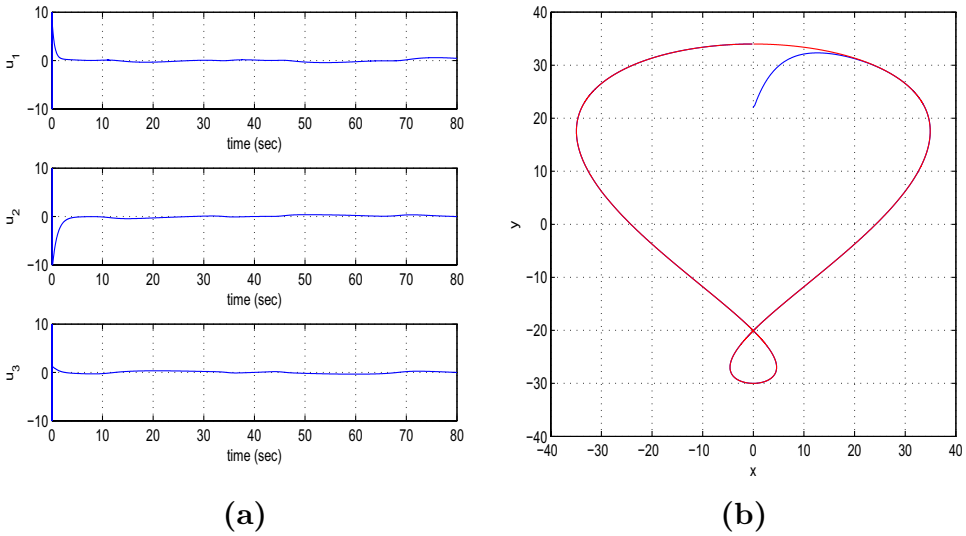

Fig. 16 Tracking of setpoint 7 for the 3-DOF USV **a** control inputs u_1 to u_3 applied to the propulsion and steerin system of the USV, **b** tracking of the reference path (red line) by the USV (blue line) in the *xy* plane

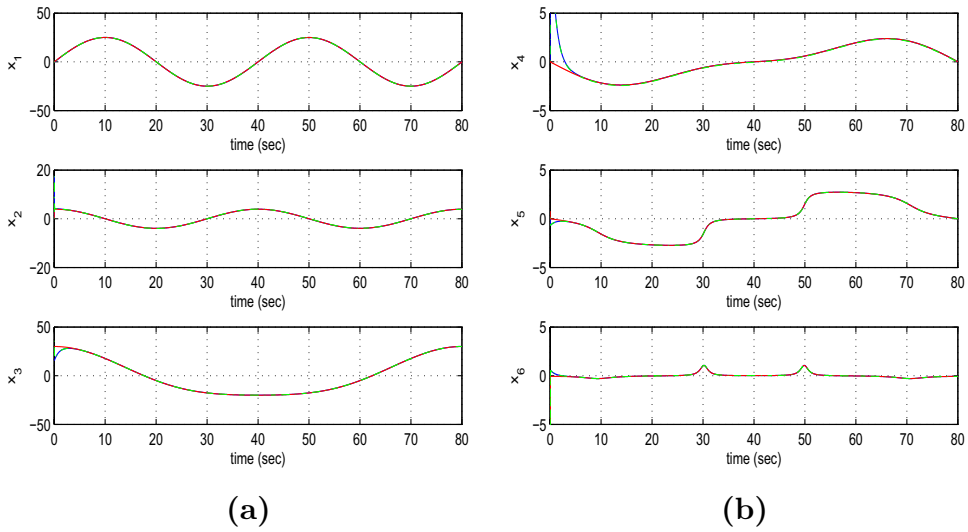

Fig. 17 Tracking of setpoint 8 for the 3-DOF USV **a** convergence of state variables x_1 to x_3 to their reference setpoints (red line: setpoint, blue line: real value, green line: estimated value), **b** convergence of state variables x_4 to x_6 to their reference setpoints (red line: setpoint, blue line: real value, green line: estimated value)

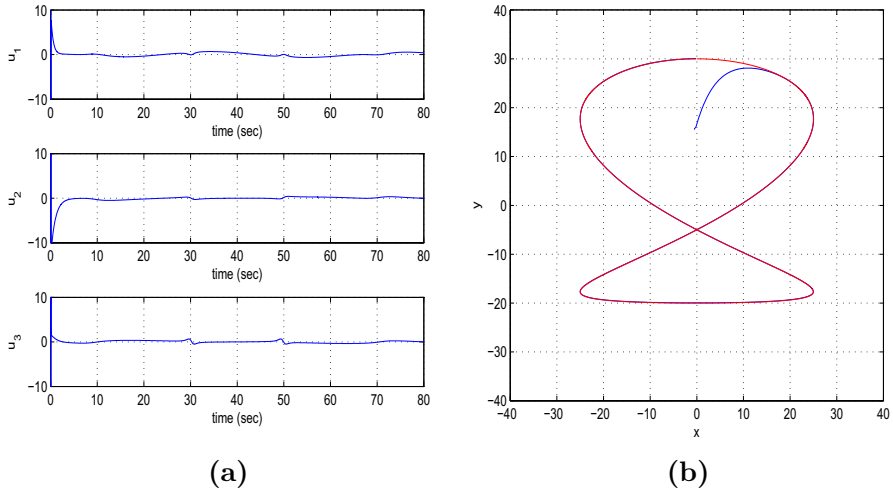

Fig. 18 Tracking of setpoint 8 for the 3-DOF USV **a** control inputs u_1 to u_3 applied to the propulsion and steering system of the USV, **b** tracking of the reference path (red line) by the USV (blue line) in the xy plane

the related reference setpoints are shown in red. Distance is measured in meters (m), angles in rad and time in sec. It can be noticed that in all cases, the proposed H-infinity controller achieved fast and accurate tracking of the reference paths under moderate variations of the control inputs.

It is noted that the transient performance of the control method depends of the selection of parameters r, ρ and Q which appear in the Riccati equation of Eq. (71). It can noticed that relatively small values of r result in elimination of the tracking error while relatively large values of matrix Q result in fast convergence to the reference setpoint. Moreover, coefficient ρ affects the robustness of the control loop. The smallest value of ρ for which one can obtain a valid solution from the algebraic Riccati equation of Eq. (71) is the one that provides the control loop with maximum robustness. It is also pointed out that the use of the H-infinity Kalman Filter as a robust state estimator has allowed to implement feedback control by using measurement of only the cartesian coordinates of the USV (x, y), of its heading angle ψ, and of the heading angle's change rate $\dot{\psi}$.

The advantages from the application of the proposed nonlinear optimal control method are outlined as follows: (i) unlike global linearization-based control schemes, the proposed nonlinear optimal control method does not require changes of variables (diffeomorphisms) and application of complicated transformations of the system's state-space model (ii) the new optimal control method is applied directly on the initial nonlinear model of the 3-DOF USV and avoids inverse transformations which are met in global linearization-based control and which may come against singularities, (iii) for the case of multivariable electromechanical systems, as for instance the USV, finding global linearization transformations is a non-trivial problem which the proposed control method avoids (iv) unlike NMPC approaches, the proposed control method is of proven convergence and stability, (v) unlike sliding-mode control approaches, the

proposed control method does not rely on intuitive definition of sliding surfaces and does not need prior transformation of the state-space model into the canonical form. (vi) unlike backstepping control, the nonlinear optmal control method does not require the state-space model of the USV to be found in the backstepping integral (triangular) form, (vii) unlike PID control, the selection of the control gains of the nonlinear optimal control scheme avoids heuristics while the reliable performance of the control loop is ensured at changes of operating points (viii) unlike multiple local models-based linearization methods, in the nonlinear optimal control approach there is no need to define multiple linearization points or to solve multiple Riccati equations and Linear Matrix Inequalities (LMIs).Consequently, the present article's control scheme is computationally more efficient.

To elaborate on the tracking performance and on the robustness of the proposed nonlinear optimal control method for the dynamics of the 3-DOF unmanned surface vessel the following Tables are given: (i) Table 1 which provides information about the accuracy of tracking of the reference setpoints by the state variables of the 3-DOF USV's state-space model, (ii) Table 2 which provides information about the robustness of the control method to parametric changes in the model of the 3-DOF USV's dynamics (change in the USV's inertia matrix coefficient m_{33}) , (iii) Table 3 which provides information about the precision in state variables' estimation that is achieved by the H-infinity Kalman Filter, (iv) Table 4 which provides the convergence times of the 3-DOF USV's state variables to the associated setpoints.

Finally, the global stability propoerties of the nonlinear optimal control method for the dynamic model of the 3-DOF

Table 1 Tracking RMSE for the 3-DOF USV in the disturbance-free case $\cdot 10^{-3}$

	$RMSE_{x_1}$	$RMSE_{x_2}$	$RMSE_{x_3}$	$RMSE_{x_4}$	$RMSE_{x_5}$	$RMSE_{x_6}$
setpoint_1	0.1118	0.1159	0.3208	0.2165	0.0813	0.0376
setpoint_2	0.0543	0.0513	0.1214	0.1146	0.1809	0.0539
setpoint_3	0.0571	0.0549	0.0809	0.1045	0.1634	0.0655
setpoint_4	0.3185	0.2837	0.0304	0.0823	0.1962	0.0553
setpoint_5	0.1489	0.0295	0.0870	0.0839	0.1511	0.0655
setpoint_6	0.1350	0.0333	0.1809	0.1131	0.1426	0.0607
setpoint_7	0.1766	0.0982	0.2298	0.0239	0.0856	0.0344
setpoint_8	0.3202	0.2415	0.1053	0.0525	0.2356	0.1001

Table 2 Tracking RMSE for the 3-DOF USV in the case of disturbances $\cdot 10^{-3}$

$\Delta a\%$	$RMSE_{x_1}$	$RMSE_{x_2}$	$RMSE_{x_3}$	$RMSE_{x_4}$	$RMSE_{x_5}$	$RMSE_{x_6}$
0%	0.0543	0.0513	0.1214	0.1146	0.1809	0.0539
10%	0.0638	0.0603	0.1767	0.1147	0.1809	0.0639
20%	0.0690	0.0689	0.2418	0.1147	0.1810	0.0639
30%	0.1002	0.0308	0.0973	0.1145	0.1812	0.0639
40%	0.0825	0.0874	0.3722	0.1148	0.1812	0.0639
50%	0.0641	0.0571	0.1728	0.1147	0.1809	0.0639
60%	0.0585	0.0643	0.2106	0.1147	0.1810	0.0639

Table 3 RMSE for the estimation performed by the H-infinity KF $\cdot 10^{-4}$

	$RMSE_{x_1}$	$RMSE_{x_2}$	$RMSE_{x_3}$	$RMSE_{x_4}$	$RMSE_{x_5}$	$RMSE_{x_6}$
setpoint_1	0.1268	0.1343	0.7427	0.9910	0.1252	0.1802
setpoint_2	0.2625	0.3274	0.1874	0.2691	0.0301	0.0392
setpoint_3	0.2078	0.3462	0.6290	0.8025	0.1145	0.1501
setpoint_4	0.0570	0.0973	0.2067	0.2829	0.0645	0.0483
setpoint_5	0.0412	0.0602	0.2213	0.2802	0.0643	0.0791
setpoint_6	0.0755	0.0746	0.1661	0.2456	0.0600	0.0513
setpoint_7	0.0462	0.0294	0.0323	0.0021	0.0342	0.0210
setpoint_8	0.1370	0.6722	0.1626	0.9890	0.1250	0.1230

Table 4 Convergence time (sec) for the 3-DOF USV's state variables

	$T_s\, x_1$	$T_s\, x_2$	$T_s\, x_3$	$T_s\, x_4$	$T_s\, x_5$	$T_s\, x_6$
setpoint_1	0.2	2.0	3.0	6.0	2.0	2.0
setpoint_2	0.2	0.2	3.0	5.0	3.0	3.0
setpoint_3	0.2	0.2	4.0	5.0	3.0	3.0
setpoint_4	0.2	1.0	2.0	5.0	3.0	3.0
setpoint_5	0.2	0.2	1.0	5.0	3.0	3.0
setpoint_6	0.2	0.2	1.0	5.0	3.0	3.0
setpoint_7	0.2	0.2	3.0	6.0	3.0	3.0
setpoint_8	0.2	0.2	4.0	6.0	3.0	3.0

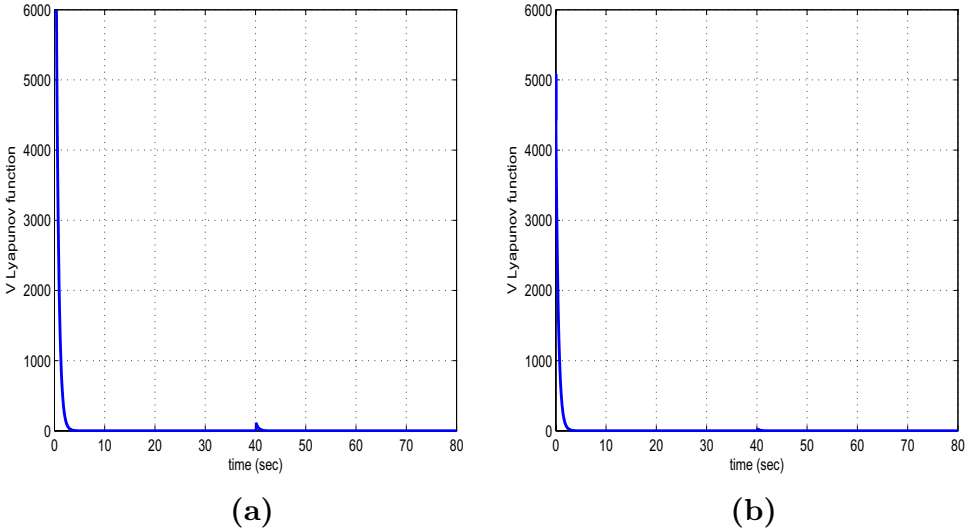

Fig. 19 Variations of the Lyapunov function of the 3-DOF USV's control loop **a** when tracking setpoint 1, **b** when tracking setpoint 2

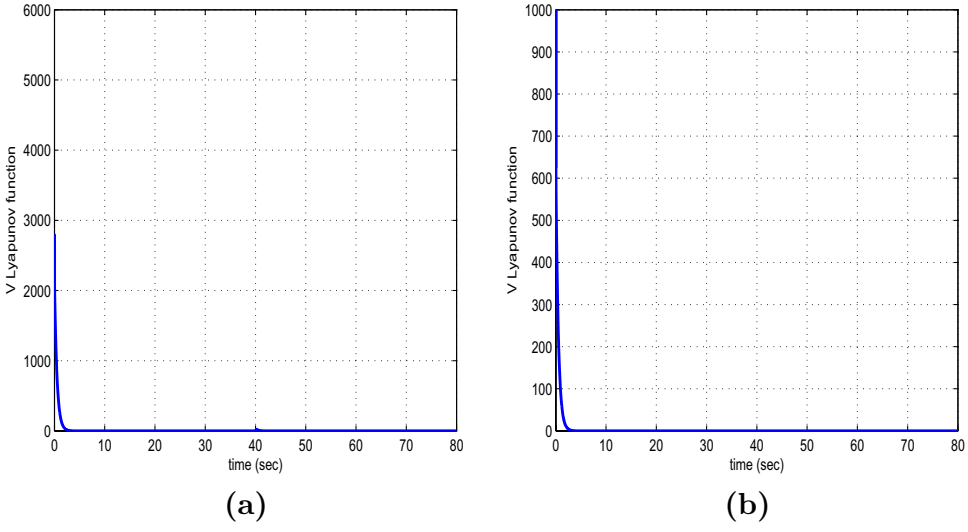

Fig. 20 Variations of the Lyapunov function of the 3-DOF USV's control loop **a** when tracking setpoint 3, **b** when tracking setpoint 4

USV are further confirmed through the following diagrams in Figs. 19, 20, 21 and 22 depicting the variations of the control system's Lyapunov function.

6 Conclusions

Autonomous navigation for Unmanned Surface Vessels (USVs) depends on the solution of the related nonlinear

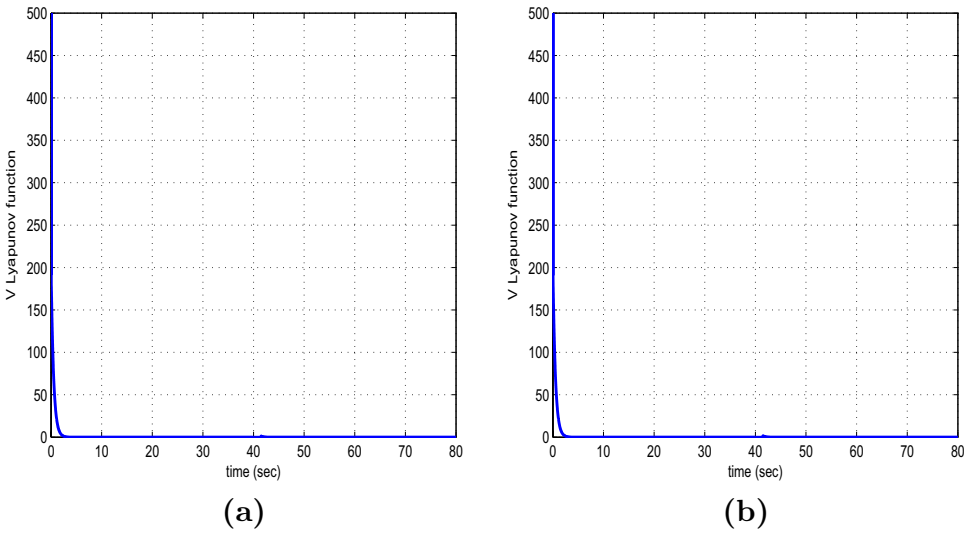

Fig. 21 Variations of the Lyapunov function of the 3-DOF USV's control loop **a** when tracking setpoint 5, **b** when tracking setpoint 6

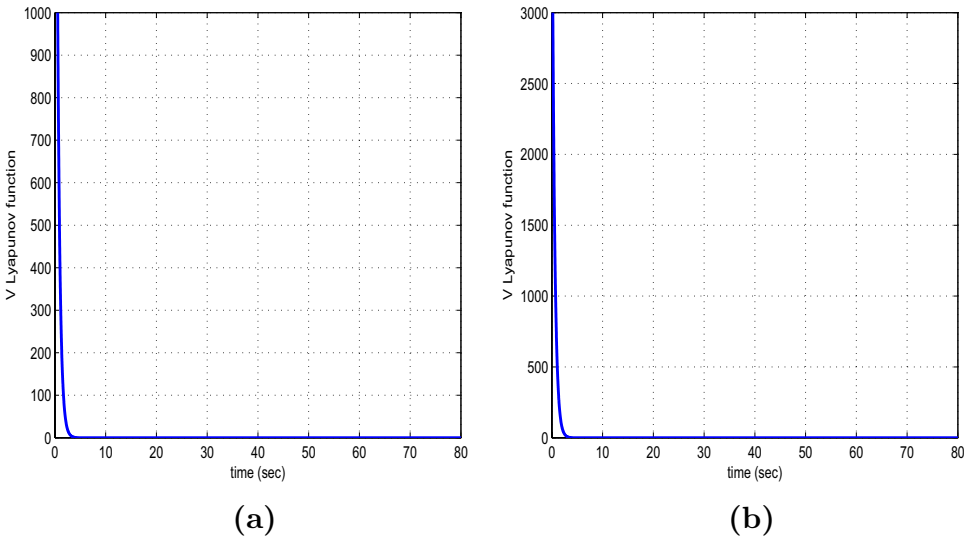

Fig. 22 Variations of the Lyapunov function of the 3-DOF USV's control loop **a** when tracking setpoint 7, **b** when tracking setpoint 8

control problem. To this end, a new nonlinear optimal control method for 3-DOF USVs has been proposed. The method relies on approximate linearization of the dynamic model of the 3-DOF USVs through Taylor series expansion and the computation of the associated Jacobian matrices. This linearization process takes place at each iteration of the control algorithm, around a temporary operating point. The operating point is dynamically updated at each sampling period and is defined by the present value of the system's state vector and by the last sampled value of the control inputs vector. The modelling error which is due to truncation of higher-order terms from the Taylor series expansion is treated as a perturbation which is dynamically updated by the robustness of the control algorithm. For the approximately linearized model of the system, a stabilizing H-infinity (optimal) feedback controller is designed.

The proposed H-infinity feedback controller achieves the solution of the optimal control problem for the dynamic model of the 3-DOF USV under model uncertainty and external perturbations. Actually, it represents the solution of a min-max differential game in which the controller tries to minimize a quadratic cost function of the state vector's tracking error, whereas the model uncertainty and external perturbation terms try to maximize this cost function. To compute the stabilizing feedback gains of the H-infinity controller, an algebraic Riccati equation is repetitively solved at each time-step of the control algorithm. The global asymptotic stability properties of the control scheme are proven through Lyapunov analysis. Furthermore, to implement state estimation-based control without the need to measure the entire state vector of the 3-DOF USV, the H-infinity Kalman Filter is used as a robust state estimator. The proposed nonlinear optimal control method for USVs retains the known

advantages of linear optimal control, that is fast and accurate tracking of reference setpoints under moderate variations of the control inputs.

The solution of the nonlinear optimal control problem for unmanned vessels allows for keeping small the ranges of the vessel's control inputs. Consequently, it allows for reducing energy consumption and thus it permits to improve the vessels' autonomy and operational capacity.The article's nonlinear optimal control method is suitable for all types of drones and autonomous vehicles, that is UGVs, AUVs, USVs and AUVs. The aim is to extend the use of the proposed nonlinear optimal control method to more types unmanned surface vessels and to more types of autonomous underwater vessels. So far the method has been used in 3-DOF unmanned surface vessels, 3-DOF autonomous underactuated hovercrafts, the 2-DOF dynamics of diving submarines, and 3-DOF autonomous underwater vessels. The method's use can be easily extended to 6-DOF autonomous underwater submarines and is particularly suitable for cases of underactuation. It can be also used for coordination and synchronization of fleets of USVs and AUVs.

Author contributions The contribution of the members of the research team is indicated by their order of appearance in the list of authors

Funding This research work has been partially supported by Grant "Ref. 3671" - "Control and estimation of dynamical nonlinear and PDE systems" of the Unit of Industrial Automation of the Industrial Systems Institute

Data availability Data about this research work are available upon reasonable request

Code availability (software application or custom code) Source code is subject to confidentiality constraints but software applications can be demonstrated upon reasonable request

Declarations

Conflict of interest No conflict of interest exists with third parties about the content of the present article

References

1. G. Rigatos, K. Busawon, *Robotic Manipulators and Vehicles: Control, Estimation and Filtering* (Springer, Berlin, 2018)
2. N. Wang, H.R. Karimi, Successive waypoints tracking of an underactuated surface vessel. IEEE Trans. Ind. Inform. **16**(2), 898–908 (2020)
3. Y. Fang, E. Zergeroglou, M.S. de Queiroz, D.M. Dawson, Global output feedback control of dynamically positioned surface vessels: an adaptive control approach. Mechatronics **14**, 341–356 (2004)
4. L. Chen, C. Yang, W. Yan, Adaptive neural network control of underactuated surface vessels with guaranteed transient performance: theory and experimental results. IEEE Trans. Ind. Electron. **67**(5), 4024–4035 (2020)
5. H. Huang, M. Gang, Y. Zhang, S. Sharma, D. Xu, A new guidance law for trajectory tracking of an underactuated unmanned surface vehicle with parameter perturbations. Ocean Eng. **175**, 217–22 (2019)
6. H. Qin, C. Li, Y. Sun, X. Li, Y. Du, Z. Ding, Finite-time trajectory tracking control of unmanned surface vessel with error constraints and input saturation. J. Franklin Inst. **357**(16), 11472–11495 (2020)
7. T. Yang, Y. Guo, Y. Zhou, S. Wen, Joint communication and control for small underactuated USV based on mobile computing technology. IEEE Access **7**, 160610–160622 (2019)
8. X. Xiang, C. Yu, Q. Zhang, P.A. Wilson, G. Xu, Maneuvering-based actuation evaluation of an AUV with control surfaces and through body thrusters. Appl. Ocean Res. **96**, 102046–102052 (2020)
9. B. Qiu, G. Wang, Y. Fan, Predictor LOS-based trajectory linearization control for path following of underactuated unmanned surface vehicles with input saturation. Ocean Eng. **214**, 107874–107885 (2020)
10. G. Gao, Y. Hen, H. Yu, J. Qin, Spatial path following control of underactuated AUV with multiple uncertainties and input saturation. IEEE Access **7**, 98014–98022 (2019)
11. B.S. Park, S.J. Yoo, An error transformation approach connectivity preserving and collision-avoidance formation tracking of networked uncertain underactuated surface vessels. IEEE Trans. Cybern. **49**(8), 2955–2966 (2019)
12. X. Liang, X. Qu, Y. Hou, Y. Li, R. Zhang, Distributed coordinated tracking control of multiple unmanned surface vehicles under complex marine environments. Ocean Eng. **205**, 107328–107336 (2020)
13. X. Liang, X. Qu, N. Wang, Y. Li, R. Zhang, Swarm control with collision avoidance for multiple underactuated surface vehicles. Ocean Eng. **191**, 106616–106625 (2019)
14. Z. Chen, Y. Zhang, Y. Nie, J. Tang, S. Zhu, Adaptive sliding-mode control design for nonlinear unmanned surface vessel using RBFNN and Disturbance Observer. IEEE Access **8**, 45457–45467 (2020)
15. N.A. Ali-Hussain, S.S. Azhar Ali, M. Ovinis, M.R. Aeshad, U.M. Al-Saggaf, Underactuated coupled nonlinear adaptive control synthesis using U-Model for multivariable Unmanned Marine Robots. IEEE Access **8**, 1851–1865 (2020)
16. X. Chen, Z. Liu, J. Zhang, D. Zhou, J. Dong, Adaptive sliding-mode path-following control system of the underactuated USV under the influence of ocean currents. IEEE J. Syst. Eng. Electron. **29**(6), 1271–1283 (2018)
17. R. Rout, R. Cui, Z. Han, Modified line-of-sight guidance law with adaptive neural network control of underactuated marine vehicle with state and input constraints. IEEE Trans. Control Syst. Technol. **28**(5), 1902–1914 (2020)
18. Z.W. Liu, H. Hou, Y.W. Wang, *Formation Containment Control of Multiple Underactuated Vessels with Sampling Communication via Hierarchical Sliding-Mode Approach* (ISA Transactions, Elsevier, Amsterdam, 2020)
19. C. Hu, R. Wang, F. Yan, N. Chen, Robust composite nonlinear feedback path-following control for underactuated surface vessels with desired-heading amendment. IEEE Trans. Ind. Electron. **69**(10), 6386–6395 (2016)
20. Y. Zhou, X. Qi, A. Incecik, Y. Ma, Z. Li, Broken lines path-following algorithm for a water-jet propulsion USV with disturbance uncertainties. Ocean Eng. **21**, 107118–107128 (2020)
21. H.N. Esfahani, R. Szlapczynski, H. Gaemi, High-performance super-twisting sliding-mode control of a maritime autonomous surface ship (MASS) using ADP-based adaptive gain and time-delay estimation. Ocean Eng. **191**, 106526–106544 (2019)
22. M. Li, C. Guo, H. Yu, Filtered extended state observer-based line-of-sight guidance for path following for unmanned surface

vehicles with unnown dynamics and disturbances. IEEE Access **7**, 178401–178412 (2019)
23. N. Wang, Z. Sun, J. Yin, Z. Zou, S.F. Su, Fuzzy unknown observer-based robust adaptive path-following control of underactuated surface vehicles subject to multiple unknowns. Ocean Eng. **176**, 57–64 (2019)
24. N. Wang, S.F. Su, Finite-time unknown observer-based interactive trajectory tracking control of asymmetric underactuated surface vehicles. IEEE Trans. Control Syst. Technol. (2021)
25. H.C. Lamraoui, Z. Qidan, Y. Bouzid, Improved active disturbance rejecter control for trajectory tracking of unmanned surface vessel. J. Mar. Sci. Ocean Technol. **17**, 18–26 (2022)
26. K. Tiwari, P. Krishnankutty, Dynamic positioning of an oceanographic research vessel using fuzzy logic controller in different sea states. J. Mar. Sci. Ocean Technol. **16**, 221–236 (2021)
27. M. Alexandersson, D. Zhang, W. Mao, R. Ringberg, A comparison of ship maneuverability models for approximate ship navigation trajectories. Ships Offshore Struct. **18**(4), 550–557 (2022)
28. H. Cao, R. Xu, S. Zhao, M. Li, X. Song, H. Dai, Robust trajectory tracking for fully input-bounded actuated unmanned surface vessel with stochastic disturbances: an approach by the homogeneous nonlinear extended state observer and dynamic surface control. Ocean Eng. **243**, 110313–110342 (2022)
29. N. Feng, D. Wu, H. Yu, A.S. Yamashita, Y. Huang, Predictive compensator-based event-triggered model predictive control with nonlinear disturbance observer for unmanned surface vehicle under cyber-attacks. Ocean Eng. **259**, 111868–11889 (2022)
30. Z. Shen, Q. Wang, S. Dong, H. Yu, Dynamic surface control for tracking of unmanned surface vessel with prescribed performance and asymmetric time-varying full-state constraints. Ocean Eng. **253**, 111319–111332 (2022)
31. G. Bejarano, J.M. Mangano, J.R. Salvador, D. Lima, Nonlinear model predictive control-based guidance low for path following. Ocean Eng. **258**, 12022–12035 (2023)
32. G. Rigatos, P. Siano, C. Cecati, A new nonlinear H-infinity feedback control approach for three-phase voltage source converters. Electr. Power Compon. Syst. **44**, 302–312 (2015)
33. G.G. Rigatos, S.G. Tzafestas, Extended Kalman filtering for fuzzy modelling and multi-sensor fusion. Math. Comput. Model. Dyn. Syst. **13**, 251–266 (2007)
34. M. Basseville, I. Nikiforov, *Detection of Abrupt Changes: Theory and Applications* (Prentice-Hall, Englewood Cliffs, 1993)
35. G. Rigatos, Q. Zhang, Fuzzy model validation using the local statistical approach. Fuzzy Sets Syst. **60**(7), 882–904 (2009)
36. G.G. Rigatos, *Modelling and Control for Intelligent Industrial Systems: Adaptive Algorithms in Robotics and Industrial Engineering* (Springer, Berlin, 2011)
37. G. Rigatos, *Nonlinear Control and Filtering Using Differential Flatness Approaches: Applications to Electromechanical Systems* (Springer, Berlin, 2015)
38. G. Rigatos, E. Karapanou, *Advances in Applied Nonlinear Optimal Control* (Cambridge Scholars Publications, Cambridge, 2020)
39. G.J. Toussaint, T. Basar, F. Bullo, H_∞ optimal tracking control techniques for nonlinear underactuated systems, in Proceedings of the IEEE CDC 2000, 39th IEEE Conference on Decision and Control, Sydney Australia (2000)
40. B.P. Gibbs, *Advanced Kalman Filtering, Least Squares and Modelling: A Practical Handbook* (J. Wiley, New York, 2011)